© 2015. Published by The Company of Biologists Ltd | Journal of Cell Science (2015) 128, 3796-3810 doi:10.1242/jcs.176768

RESEARCH ARTICLE

Initiation of lamellipodia and ruffles involves cooperation between mDia1 and the Arp2/3 complex

Tadamoto Isogai[1], Rob van der Kammen[1], Daniela Leyton-Puig[2], Katarzyna M. Kedziora[2], Kees Jalink[2] and Metello Innocenti[1,*]

ABSTRACT

Protrusion of lamellipodia and ruffles requires polymerization of branched actin filaments by the Arp2/3 complex. Although regulation of Arp2/3 complex activity has been extensively investigated, the mechanism of initiation of lamellipodia and ruffles remains poorly understood. Here, we show that mDia1 acts in concert with the Arp2/3 complex to promote initiation of lamellipodia and ruffles. We find that mDia1 is an epidermal growth factor (EGF)-regulated actin nucleator involved in membrane ruffling using a combination of knockdown and rescue experiments. At the molecular level, mDia1 polymerizes linear actin filaments, activating the Arp2/3 complex, and localizes within nascent and mature membrane ruffles. We employ functional complementation experiments and optogenetics to show that mDia1 cooperates with the Arp2/3 complex in initiating lamellipodia and ruffles. Finally, we show that genetic and pharmacological interference with this cooperation hampers ruffling and cell migration. Thus, we propose that the lamellipodium- and ruffle-initiating machinery consists of two actin nucleators that act sequentially to regulate membrane protrusion and cell migration.

KEY WORDS: Arp2/3, Actin, Cell migration, Lamellipodia, mDia1, Ruffles

INTRODUCTION

Lamellipodia and ruffles are thin sheet-like membrane protrusions composed of branched actin filaments (Pollard and Borisy, 2003) assembled by the actin-related protein 2 and 3 (Arp2/3) complex, an evolutionary conserved and intrinsically inactive seven-subunit protein complex (Goley and Welch, 2006). Activation of the Arp2/3 complex requires two cofactors, a pre-existing actin filament (often referred to as mother actin filament) and a nucleation-promoting factor (NPF) (Goley and Welch, 2006; Le Clainche and Carlier, 2008; Pollard, 2007; Pollard and Borisy, 2003). Binding of these two cofactors enables the Arp2/3 complex to adopt the active conformation and nucleate a daughter actin filament from the side of the mother filament. The Wiskott–Aldrich syndrome protein (WASP) family verprolin-homologous protein (WAVE) proteins (WAVE1–WAVE3) are NPFs that have been shown to activate the Arp2/3 complex and induce the assembly of branched actin filaments *in vitro* (Goley and Welch, 2006; Le Clainche and Carlier, 2008; Pollard, 2007; Pollard and Borisy, 2003).

[1]Division of Molecular Genetics, The Netherlands Cancer Institute, Plesmanlaan 121, Amsterdam 1066 CX, The Netherlands. [2]Division of Cell Biology I, The Netherlands Cancer Institute, Plesmanlaan 121, Amsterdam 1066 CX, The Netherlands.

*Author for correspondence (m.innocenti@nki.nl)

Received 1 July 2015; Accepted 2 September 2015

WAVE proteins form a stable complex with four other proteins (Gautreau et al., 2004; Innocenti et al., 2004), namely Abi-1 (or its paralogs Abi-2 and Abi-3), Nap1 (Nck-associated protein 1, also known as NCKAP1) [or its paralog HEM1(NCKAP1L)], PIR121 (also known as CYFIP2) (or its paralog Sra-1, CYFIP1) and HSPC300 (also known as BRK1) (Takenawa and Suetsugu, 2007). Physical binding between activated Rac and PIR121/Sra-1 allows the WAVE complex to translate Rac signals directly into Arp2/3-complex-dependent actin polymerization (Innocenti et al., 2004; Lebensohn and Kirschner, 2009). Knockdown or knockout of either WAVE complex subunit abrogates lamellipodium and ruffle formation (Beli et al., 2008; Innocenti et al., 2004; Yamazaki et al., 2003; Yan et al., 2003), as well as phagocytosis and macropinocytosis (Innocenti et al., 2005; Mercer and Helenius, 2009; Suetsugu et al., 2003). As depletion of the Arp2/3 complex causes similar defects (Beli et al., 2008; Rotty et al., 2013; Suraneni et al., 2012), the WAVE and the Arp2/3 complexes are crucial components of the lamellipodium- and ruffle-making machinery.

Formin proteins represent a different class of actin nucleators as they promote the polymerization of linear actin filaments (Chesarone et al., 2010; Pollard, 2007). Formins are defined by an evolutionary conserved signature consisting of juxtaposed formin homology (FH) 1 and FH2 domains: the FH1 domain binds the G-actin-binding protein profilin thereby modulating how the flanking FH2 domain affects actin filament nucleation and elongation (Kovar et al., 2006; Romero et al., 2004).

Human and mouse diaphanous 1 [DIAPH1 and mDia1 (also known as DIAP1), respectively] are orthologous formins collectively referred to as mDia1. mDia1 bears a diaphanous inhibitory domain (DID) and a diaphanous auto-regulatory domain (DAD) enclosing the FH1 and FH2 domains at the N-terminal and C-terminal side, respectively (Schonichen and Geyer, 2010). Interaction between the DID and DAD keeps mDia1 auto-inhibited and is disrupted when activated Rho binds the GTPase-binding domain located just upstream of the DID (Otomo et al., 2005). Consistent with being activated by Rho, mDia1 also acts as a Rho effector, regulating actin-dependent processes (Chesarone et al., 2010; Kim et al., 2009). mDia1 is a component of the phagocytosis cup (Brandt et al., 2007; Colucci-Guyon et al., 2005; Lewkowicz et al., 2008) and might also localize at the leading edge of migrating cells and within ruffles (Kurokawa and Matsuda, 2005; Watanabe et al., 1997; Zaoui et al., 2008).

The Arp2/3-complex activation mechanism and the proteins composing the lamellipodium- and ruffle-making machinery are sufficient to faithfully describe the mechanism that sustains expansion of lamellipodia and ruffles (Bugyi and Carlier, 2010; Insall and Machesky, 2009; Le Clainche and Carlier, 2008; Pollard and Borisy, 2003). In addition, recent studies have identified inhibitory proteins for the Arp2/3 complex and have elucidated the mechanisms that cause retraction of lamellipodia and ruffles (Chan

Journal of Cell Science

Journal of Cell Science (2015) 128, 3796-3810 doi:10.1242/jcs.176768

et al., 2011; Dang et al., 2013). However, we still ignore the mechanism of initiation of lamellipodia and ruffles because the origin and availability of the pre-existing mother filaments mediating initial activation of the Arp2/3 complex remain unknown.

In this study, we have employed a multi-disciplinary approach to show that mDia1 polymerizes linear actin filaments for initial activation of the Arp2/3 complex within nascent lamellipodia and ruffles. The finding that mDia1 plays an essential role in the mechanism of initiation of lamellipodia and ruffles shows that the lamellipodium- and ruffle-initiating machinery consists of two actin nucleators that act sequentially to regulate membrane protrusion and cell migration.

RESULTS

mDia1 is involved in formation of membrane ruffles

We found that endogenous mDia1 localized in epidermal growth factor (EGF)-induced ruffles and is the formin protein that shows the highest expression in HeLa cells (Fig. S1A,B, and see below). On this ground, we decided to study the contribution of mDia1 to the formation of lamellipodia and ruffles. We used two different *DIAPH1*-targeting short hairpin RNAs (shRNAs) to generate stable mDia1-knockdown HeLa cells: hairpin #1 and #2 reduced mDia1 protein levels by 89±4% and 94±2% (mean±s.d.; n=3), respectively, without affecting the expression of EGFR, mDia2, the WAVE complex subunits WAVE2, WAVE1, Nap1 and Pir121, and the Arp2/3-complex subunits ARPC2 and ARPC3 (Fig. 1A). Likewise, morphology of control and mDia1-knockdown cells at the steady state was essentially identical (data not shown).

Although control and mDia1-knockdown HeLa cells attained similar Rho and Rac1 activities both in resting conditions and upon EGF stimulation (Fig. 1B,C), the cells depleted of mDia1 did not ruffle upon EGF addition and formed filopodium-like protrusions (Fig. 1D,E; Table S1). This response is remarkably similar to that of Nap1-knockdown cells, which retain only residual WAVE complex levels, and Arp2/3-complex-knockdown cells (Beli et al., 2008). Time-lapse video microscopy showed that the actin-rich, ruffle-like and filopodia-like structures observed in control and mDia1-knockdown HeLa cells are dynamic protrusions of the plasma membrane that grow by extension (Fig. 1F; Movies 1, 2). Established markers of lamellipodia and ruffles (ARPC2 and WAVE2) and filopodia (fascin) confirmed that EGF triggers the formation of genuine ruffles and filopodia in control and mDia1-knockdown cells, respectively (Fig. S1C,D). Thus, the suggested role of mDia1 in the making of filopodia (Goh et al., 2011) is either non-essential or cell-type specific. In addition, mDia1 downregulation impaired membrane ruffling in MDA-MB-231 (Fig. S2A–C) and COS-7 cells (Fig. S2D–F), thereby supporting the generality of the function of mDia1.

mDia1 is an EGF-regulated actin nucleator controlling membrane ruffling

We rescued mDia1-knockdown cells with mouse mDia1, which is highly similar to DIAPH1 but refractory to the *DIAPH1*-targeting hairpins. The cells re-expressing wild-type mDia1 showed a significant increase in EGF-induced ruffling (Fig. 2A,B; Table S2). Importantly, we ruled out that mouse mDia1 could also exert similar effects on cells that express DIAPH1 (Table S3 and data not shown). Several lines of evidence collectively support the specificity of the function of mDia1 in ruffle formation: (1) HeLa and MDA-MB-231 cells ruffle independently of mDia2 (Beli et al., 2008; and data not shown, respectively), (2) HeLa cells lack mDia3 (Isogai et al., 2015a,b; Fig. S1B), (3) RNA interference (RNAi)-mediated knockdown of mDia3 in COS-7 cells did not exert any effect on ruffling (Fig. S2D–F), and (4) overexpression of neither mDia2 nor profilin-1 rescued EGF-induced ruffling in the mDia1-knockdown cells, nor did it alter the remodeling of the actin cytoskeleton in the control cells (Fig. S3A–C, Table S4). Of note, the fact that profilin-1 had no noticeable effects in the control cells also ruled out that the downregulation of mDia1 simply perturbs the distribution of actin monomers between the lamellipodium- or ruffle- and the filopodium-making machineries (Rotty et al., 2015; Suarez et al., 2015). Moreover, the observation that mDia1 mutants lacking either the FH2 domain (mDia1ΔFH2) or the ability to bind activated Rho (mDia1 V160D) (Otomo et al., 2005) did not significantly rescue the mDia1-knockdown cells suggests that mDia1 functions as an EGF-activated actin-regulatory protein controlling membrane ruffling (Fig. S3D–F, Table S5). To further strengthen this point, we first compared free barbed ends present in control and mDia1-knockdown cells prior to and after EGF addition. In resting conditions, both cell lines showed a similar distribution and overall level of free barbed ends (Fig. 2C,D). Stimulation of the control cells with EGF caused a rapid increase in the free barbed ends (Fig. 2C,E,G). This effect was particularly evident close to the supra-basal regions of the plasma membrane, which are prospective sites of ruffle formation (Fig. 2C). In keeping with the notion that EGF signaling regulates the activity of mDia1, no significant increase in the free barbed ends could be measured in mDia1-knockdown cells after EGF stimulation (Fig. 2D,F,G). Nevertheless, stress fibers located close to the basal membrane were similar in both cell lines, thus suggesting that mDia1 and other formins act redundantly in regulating these actin-based structures. Importantly, supra-basal barbed-end formation near the plasma membrane correlated with the enrichment of endogenous mDia1 in both nascent and expanding ruffles (Fig. 3). As overexpression of the anti-capping protein Mena (Bear and Gertler, 2009) did not rescue EGF-induced ruffling in the mDia1-knockdown cells (Fig. S3G,H, Table S6), the contribution of mDia1 to membrane ruffling goes beyond actin-filament elongation and likely involves actin nucleation.

mDia1 polymerizes linear actin filaments activating the Arp2/3 complex

To test directly the above hypothesis, we purified recombinant wild-type full-length mDia1 and a mutant thereof (M1182A, hereafter MA) that should be constitutively active because the M-to-A mutation prevents the auto-inhibitory DID–DAD interaction without affecting actin nucleation (Alberts, 2001; Gould et al., 2011) (Fig. 4A). We carried out total internal reflection fluorescence microscopy (TIRFm)-based *in vitro* actin polymerization assays in the presence of profilin, which binds monomeric actin, reducing spontaneous nucleation and filament assembly *in vitro* (Kovar et al., 2006; Romero et al., 2004). Actin-bound profilin also unmasks actin nucleation and enhances filament elongation by mDia1 deletion mutants (Kovar et al., 2006; Romero et al., 2004). In line with the mDia1 auto-inhibition model, wild-type mDia1 did not affect either nucleation or elongation of actin filaments (Fig. 4B,E; Movie 3) and could be activated by GTPγS-bound RhoA (data not shown). By contrast, mDia1 MA markedly increased filament nucleation and also accelerated filament elongation (Fig. 4C–E; Fig. S3I, Movie 4). Taken together, these data indicate that full-length mDia1 is an auto-inhibited actin nucleator that controls also actin filament elongation, as previously suggested by mDia1 deletion mutants (Kovar et al., 2006; Romero et al., 2004) and quasi full-length mDia1 (Maiti et al., 2012).

Journal of Cell Science (2015) 128, 3796-3810 doi:10.1242/jcs.176768

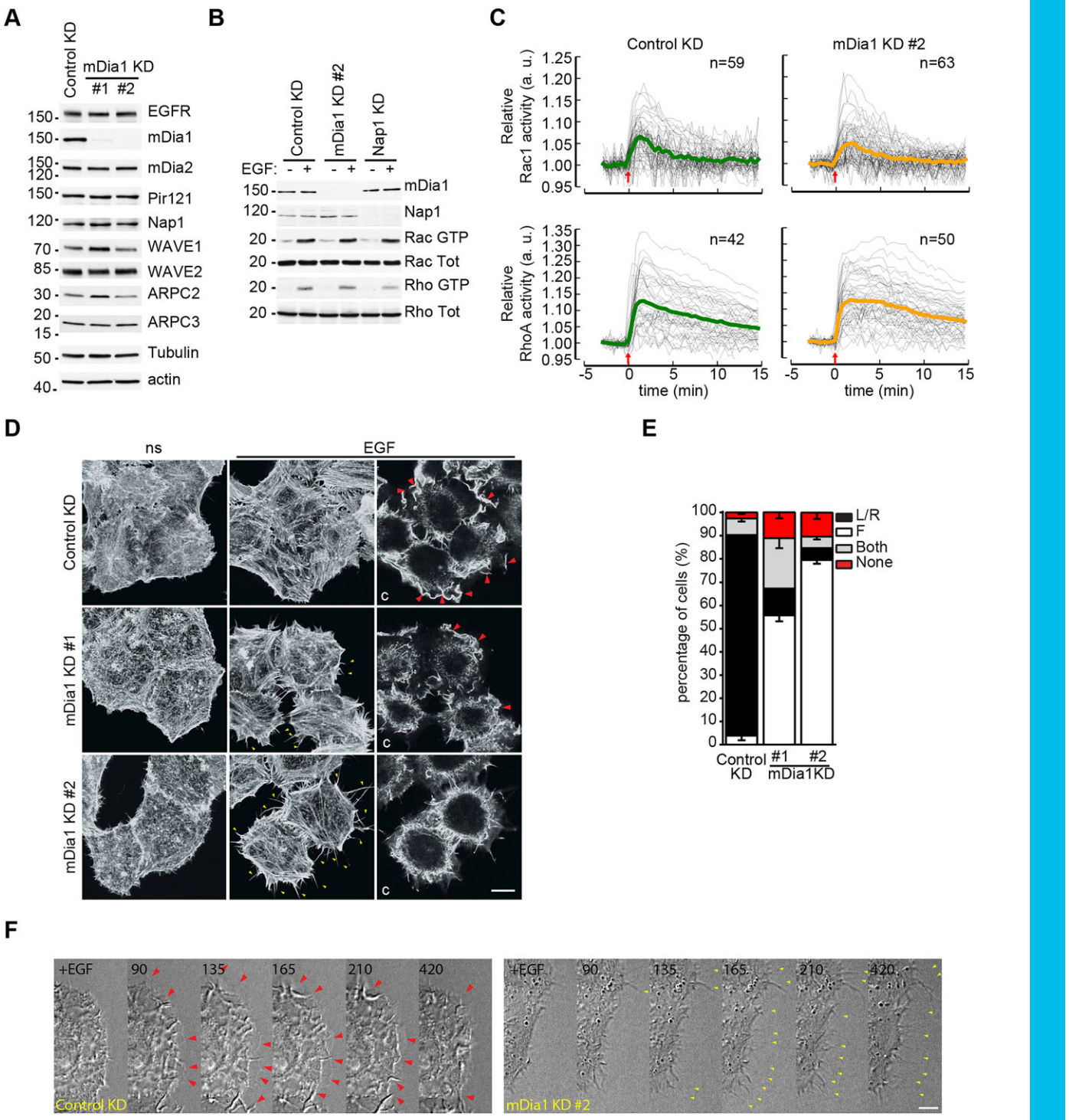

Fig. 1. mDia1 is required for EGF-induced membrane ruffling. (A) Characterization of control knockdown (KD) and mDia1 KD (#1 and #2) cells. Total cell lysates (30 µg) were compared using the indicated antibodies. One of two experiments that were performed with similar results is shown. (B) GTP-bound and total Rac1 and Rho levels are independent of mDia1. Control KD and mDia1 KD cells were serum starved and then either stimulated with EGF (100 ng ml^{-1}) for 3 min or left untreated. One of three experiments that were performed with similar results is shown. (C) Kinetics of Rac1 and Rho activity are independent of mDia1. Control KD and mDia1 KD HeLa cells transfected with either the Rac1 (top) or RhoA (bottom) biosensor. Relative Rac1 and RhoA activities are plotted as mean (coloured bold line) against time (min). Addition of EGF (100 ng ml^{-1}) is indicated with a red arrow. Two-way ANOVA analysis did not reveal any significant difference (n=42–63 from three independent experiments). (D,E) Actin cytoskeleton in control KD and mDia1 KD cells. (D) Serum-starved (ns) and EGF-stimulated (EGF, 100 ng ml^{-1}, 7 min) cells stained with TRITC–phalloidin. Yellow and red arrowheads mark filopodia and ruffles, respectively. Representative maximal projections and central confocal sections (c) are shown. Scale bar: 10 µm. (E) EGF-induced protrusions were classified and quantified as described in the Materials and Methods (L/R, lamellipodia and ruffles; F, filopodia). The graph shows mean±s.e.m. (n≥300 cells from three independent experiments, Table S1). (F) EGF induces dynamic ruffle-like and filopodia-like protrusions that grew by extension in control and mDia1-knockdown cells, respectively. Serum-starved cells were stimulated with EGF and imaged every 15 s. In the phase-contrast snapshots extracted from Movies 1 and 2, filopodia and ruffles are highlighted as in D. Scale bar: 10 µm. A high-resolution version of this figure can be downloaded at http://dx.doi.org/10.6084/m9.figshare.1554814.

Journal of Cell Science (2015) 128, 3796-3810 doi:10.1242/jcs.176768

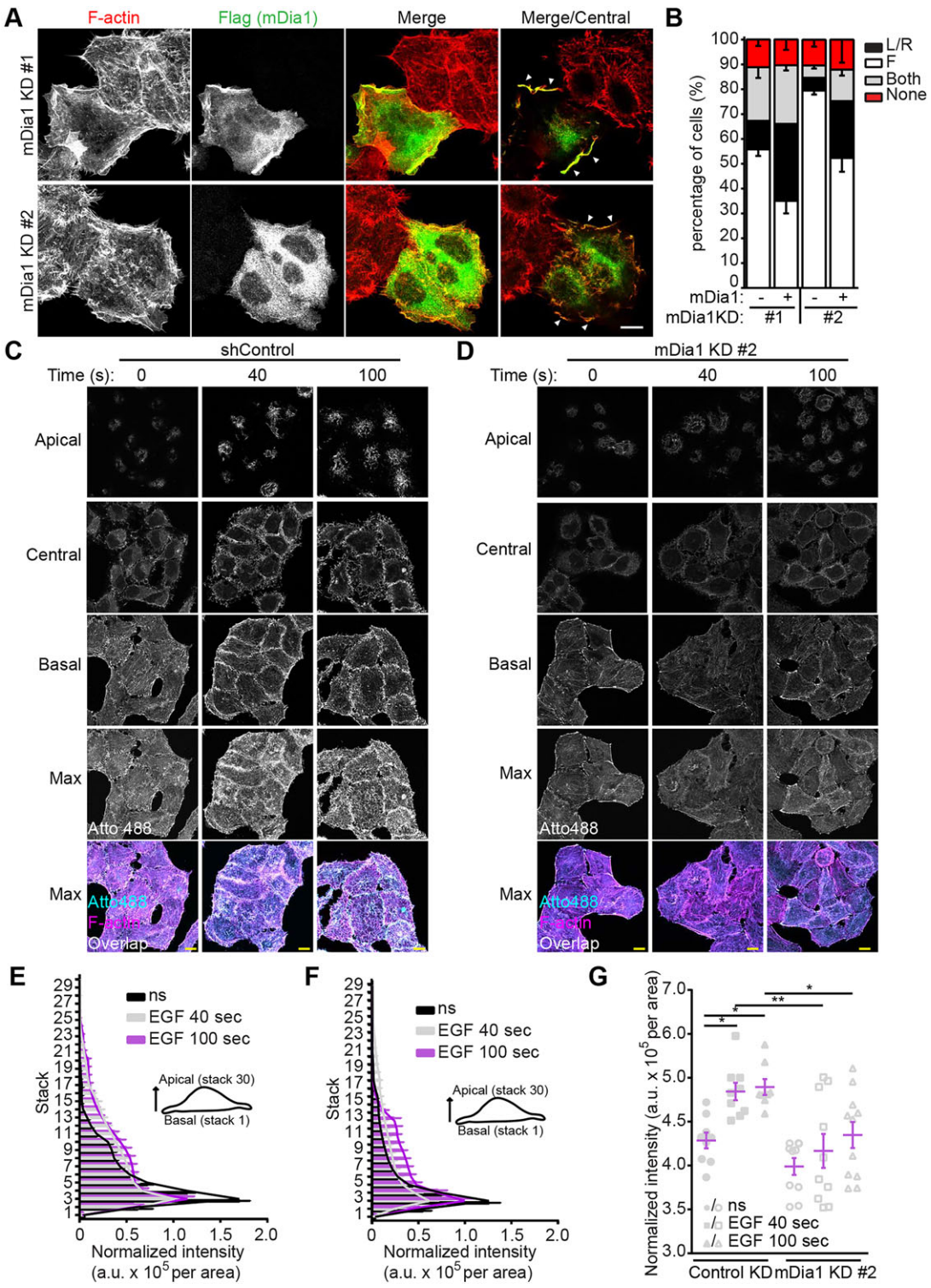

Fig. 2. See next page for legend.

Next, we combined mDia1 with WAVE2 (Fig. 4A) and the Arp2/3 complex to shed light on how mDia1 contributes to membrane ruffling. As expected, the Arp2/3 complex could nucleate branched actin filament arrays only upon activation by WAVE2 (Fig. S3J–L). However, actin nucleation by the Arp2/3 complex was severely limited by the scarcity of mother actin filaments because spontaneous self-assembly relies on free G-actin escaping the control of profilin-1. In agreement with the fact that mDia1 does not bind to the Arp2/3 complex ((Beli et al., 2008, and data not shown), mDia1 MA was unable to functionally replace WAVE2 (Fig. S3M). However, concomitant addition of mDia1 MA and WAVE2 reduced the lag time of initiation and increased the number of these arrays, thereby revealing that these two proteins synergize in activating the Arp2/3 complex (Fig. 4F,G; Movie 5). Instead, auto-inhibited wild-type

Journal of Cell Science

Fig. 2. mDia1 is required for formation of free barbed ends upon EGF stimulation. (A,B) Mouse mDia1 rescues mDia1-knockdown (KD) cells. mDia1 KD (#1 and #2) cells were transfected with Flag-tagged mDia1, serum starved and stimulated with EGF as in Fig. 1D. (A) After fixation, cells were stained with anti-Flag antibodies (green in merge) and TRITC–phalloidin (red in merge) to detect mDia1 and actin filaments, respectively. Representative maximal projections and central confocal sections (Merge/Central) are shown. White arrowheads mark lamellipodia and ruffles. Scale bar: 10 µm. (B) EGF-induced protrusions were quantified as in Fig. 1E (–, non-transfected cells; +, mDia1-expressing cells; L/R, lamellipodia and ruffles; F, filopodia). Graph shows mean±s.e.m. (n≥300 cells from three independent experiments, Table S2). (C,D) mDia1-knockdown cells contain less free barbed ends upon a short EGF treatment in comparison to control cells. Control (C) and mDia1-knockdown #2 (D) cells were serum starved overnight and stimulated with EGF (100 ng ml^{-1}) for the indicated time. Free barbed ends were labeled as described in the Materials and Methods. Representative z-stacks of basal, central and apical sections were imaged and processed using identical settings (Max, maximal projection of the z-stack). Scale bars: 10 µm. Overlap (white) between the Atto488–actin and the TRICT–phalloidin is shown in a separate maximal projection. (E,F) Distribution of free barbed ends in control (E) and mDia1-knockdown #2 (F) cells stimulated as indicated with EGF. Normalized barbed-end intensity per cell area [arbitrary units (a.u.)×10^5] was plotted per stack. The bar graph represents the mean±s.e.m. of two independent experiments and lines marks the mean (n≥11 images containing on average 8–10 cells). ns, not simulated. (G) Scatter plot of data derived from E and F. Normalized barbed-end intensity per cell area (a.u.×10^5) was calculated as described in the Materials and Methods and plotted for control and mDia1-knockdown cells. Mean±s.e.m. are indicated with pink horizontal and vertical bars, respectively. *P<0.05; **P<0.01 (one-way ANOVA with Bonferroni's multiple comparison test). A high-resolution version of this figure can be downloaded at http://dx.doi.org/10.6084/m9.figshare.1554814.

mDia1 had minor effects only at very high concentration (Fig. 4G). These results suggest that mDia1 nucleates linear actin filaments that, in combination with the NPF activity of WAVE2, are required for efficient nucleation of branched actin filaments by the Arp2/3 complex. Moreover, the dose-dependent effects of mDia1 (Fig. 4F, G) agree with the formation of mother filaments being a rate-limiting step in Arp2/3 complex activation.

mDia1 regulates initiation of lamellipodia and ruffles

To gain insight into how mDia1 and the Arp2/3 complex collaborate in the making of ruffles, we used ground state depletion (GSD) super-resolution microscopy (SRm) to map the position of endogenous WAVE2 and mDia1 within EGF-induced ruffles: when WAVE2 was enriched at the protruding front (Fig. 5A,C), mDia1 mainly populated the region behind the tip (Fig. 5B,C). The localization of WAVE2 at or close to the tip of lamellipodia and ruffles agrees with its ability to stimulate Arp2/3-complex-mediated actin polymerization and ensuing membrane protrusion. The localization of mDia1 suggests that this formin might contribute to the initiation of lamellipodia and ruffles, and be dispensable for their subsequent growth and protrusion, an autocatalytic process driven by the Arp2/3 complex. If so, mDia1 might play only an ancillary role at the tip of expanding lamellipodia and ruffles. To assess whether mDia1 is dispensable for the expansion of lamellipodia and ruffles after the initiation phase, we fused full-length mDia1 to SuperNova, a derivative of KillerRed that facilitates chromophore-assisted light inactivation (CALI) (Sano et al., 2014; Takemoto et al., 2013). First, we showed that SuperNova–mDia1 rescues ruffle formation in the mDia1-knockdown cells, almost as efficiently as Flag-tagged mDia1 (Fig. S4A,B, Table S7). Then, we verified the effectiveness of CALI and found that intense illumination of SuperNova–mDia1-expressing cells prior to EGF stimulation significantly reduced lamellipodia and ruffle formation compared to neighboring non-treated SuperNova–mDia1-expressing cells (Fig. 5D; Movie 6, Table S8). Finally, we exploited this optogenetic tool to gain spatiotemporal control of the mDia1 activity. Because we found that inactivation of SuperNova–mDia1 in the mDia1-knockdown cells that ruffled upon EGF stimulation did not arrest ruffling (Fig. 5E; Movie 7, Table S8), it appears that mDia1 is required only for initiation of lamellipodia and ruffles.

mDia1 and the Arp2/3 complex cooperate in the making of ruffles

The observed synergy between mDia1 and the Arp2/3 complex in the initiation of lamellipodia and ruffles implies that hyperactivation of either protein should compensate for the knockdown and ensuing decreased activity of the other one and rescue, at least partially, ruffling. In order to test this possibility, we exploited the fact that knockdowns retain low levels of the downregulated protein (i.e. they are equivalent to hypomorphic mutants) to carry out functional complementation assays in which we manipulated the NPF activity of the WAVE complex and the abundance of mother filaments, the two Arp2/3 complex co-activators (Fig. 6A). To forcefully augment the activity of the WAVE complex, we overexpressed constitutively active Rac1 (Rac1 Q61L) in control, mDia1- and Nap1-knockdown cells. Rac1 Q61L readily induced dorsal ruffles in control knockdown HeLa cells (Fig. 6B,C), as previously reported (Innocenti et al., 2004). Most importantly, Rac1 Q61L efficiently rescued mDia1-knockdown cells, although ruffling was slightly reduced compared to the control cells (Fig. 6B,C). This observation suggests that the action of mDia1 might extend beyond the initiation phase of lamellipodium and ruffle formation, and agrees with mDia1 localizing within these actin-based protrusions. By contrast, Nap1-knockdown cells did not ruffle upon either EGF stimulation (Beli et al., 2008; Innocenti et al., 2005) or Rac1 Q61L overexpression (Fig. 6B,C), further underlining that the WAVE complex is the main NPF acting downstream of Rac1. However, it remains possible that Rac1 Q61L activates the Arp2/3 complex through WAVE-complex-dependent pathways that are either independent of or inhibited by mDia1. To increase the mother filaments available for Arp2/3-dependent actin polymerization, we overexpressed mDia1 in Nap1-knockdown cells and partially rescued EGF-induced ruffling (Fig. 6D,E; Table S9). As (1) constitutively active Rac induced membrane ruffling and concomitant activation of endogenous Rho (Fig. 6B,C and data not shown, respectively), whereas (2) constitutively active Rho (Fig. S4C,D and Nobes and Hall, 1995) and (3) activated mDia1-deletion mutants were insufficient to trigger ruffle formation (Watanabe et al., 1999 and data not shown), the sum of these experiments shows that mDia1 and the Arp2/3 complex cooperate in the making of ruffles and do not act independently of each other.

mDia1 and the Arp2/3 complex cooperate in promoting ruffling and regulate cell motility

Ubiquitous expression of mDia1 and the WAVE complex suggests that the protein levels and activities of mDia1 and the Arp2/3 complex determine the impact of either nucleator on membrane ruffling. Consistent with this hypothesis, (1) WAVE2 attained a higher expression in COS-7 and MDA-MB-231 cells than HeLa cells (Fig. 7A) and (2) mDia1 was required for MDA-MB-231 cells to ruffle upon reduction of Arp2/3 complex activity by the small molecule CK666 (Nolen et al., 2009) (Fig. 7B,C). In keeping with the idea that cooperation between mDia1 and the Arp2/3 complex mediates EGF-induced membrane ruffling (Fig. 1D,E; Fig. S3 and Fig. 7B,C) and the crucial role of lamellipodia and ruffles in mesenchymal cell migration

Journal of Cell Science (2015) 128, 3796-3810 doi:10.1242/jcs.176768

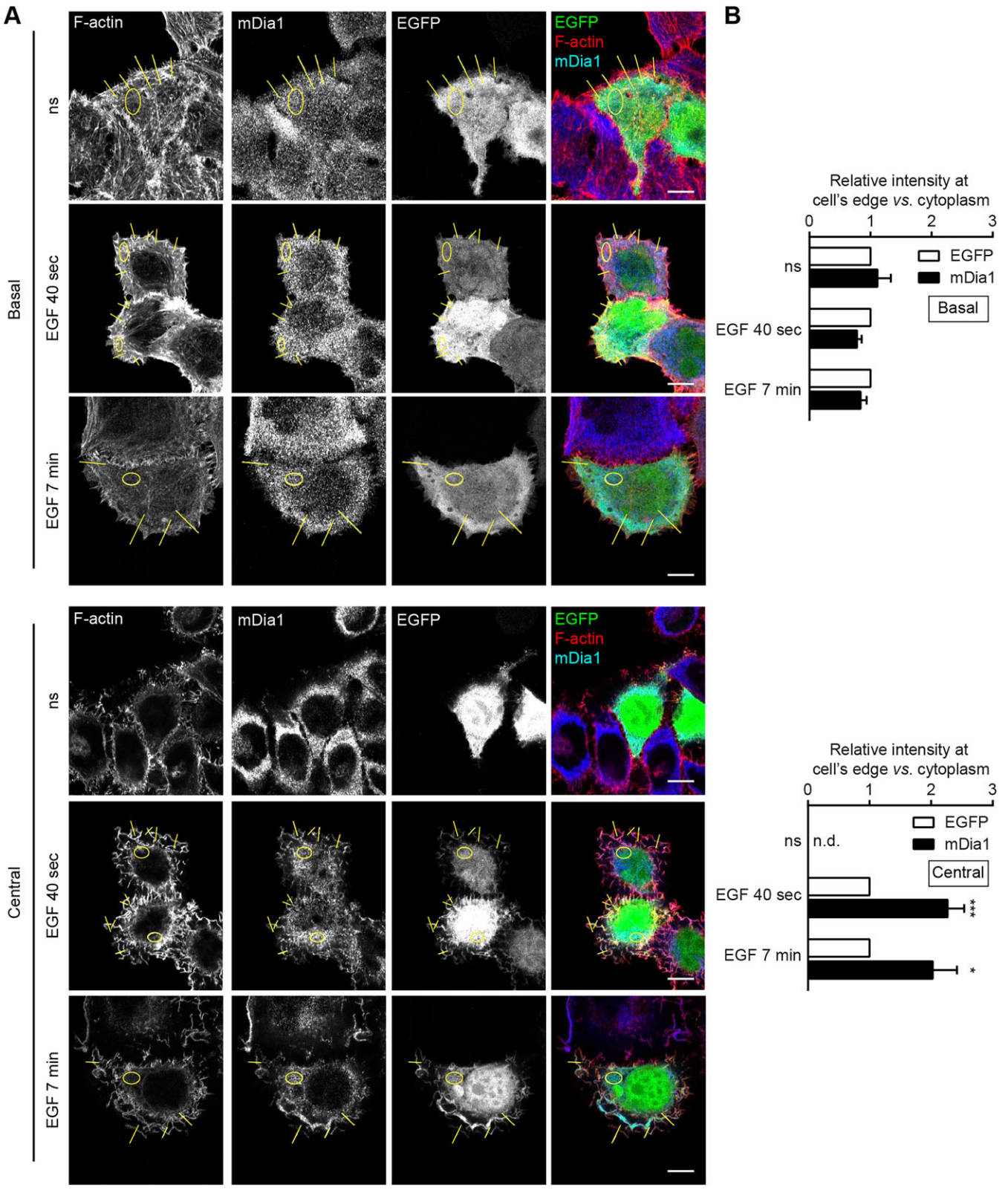

Fig. 3. Endogenous mDia1 is enriched in nascent and mature ruffles. (A) Localization of endogenous mDia1. Control knockdown (KD) HeLa cells were transfected with pEGFP encoding soluble EGFP (green in merge) as a volume marker, serum starved and stimulated with EGF for 40 s and 7 min, or left untreated (ns). After fixation, cells were stained with anti-mDia1 antibodies (blue in merge) and TRITC–phalloidin (F-actin, red in merge). Representative basal (Basal) and central (Central) confocal sections are shown. Scale bars: 10 µm. (B) Endogenous mDia1 is enriched in both nascent and mature ruffles. Line scans and circular areas were used to measure the intensity of EGFP and endogenous mDia1 at the cell edges and in the cytoplasm, respectively. The normalized relative intensity of mDia1 was calculated as described in the Materials and Methods for both basal and central sections and plotted as mean±s.e.m. **P*<0.05; ****P*<0.001 (Student's *t*-test; *n*=10–21 ruffles). As the serum-starved cells were flat and devoid of ruffles, intensity in the central sections of could not be measured (n.d., not determined). A high-resolution version of this figure can be downloaded at http://dx.doi.org/10.6084/m9.figshare.1554814.

Journal of Cell Science (2015) 128, 3796-3810 doi:10.1242/jcs.176768

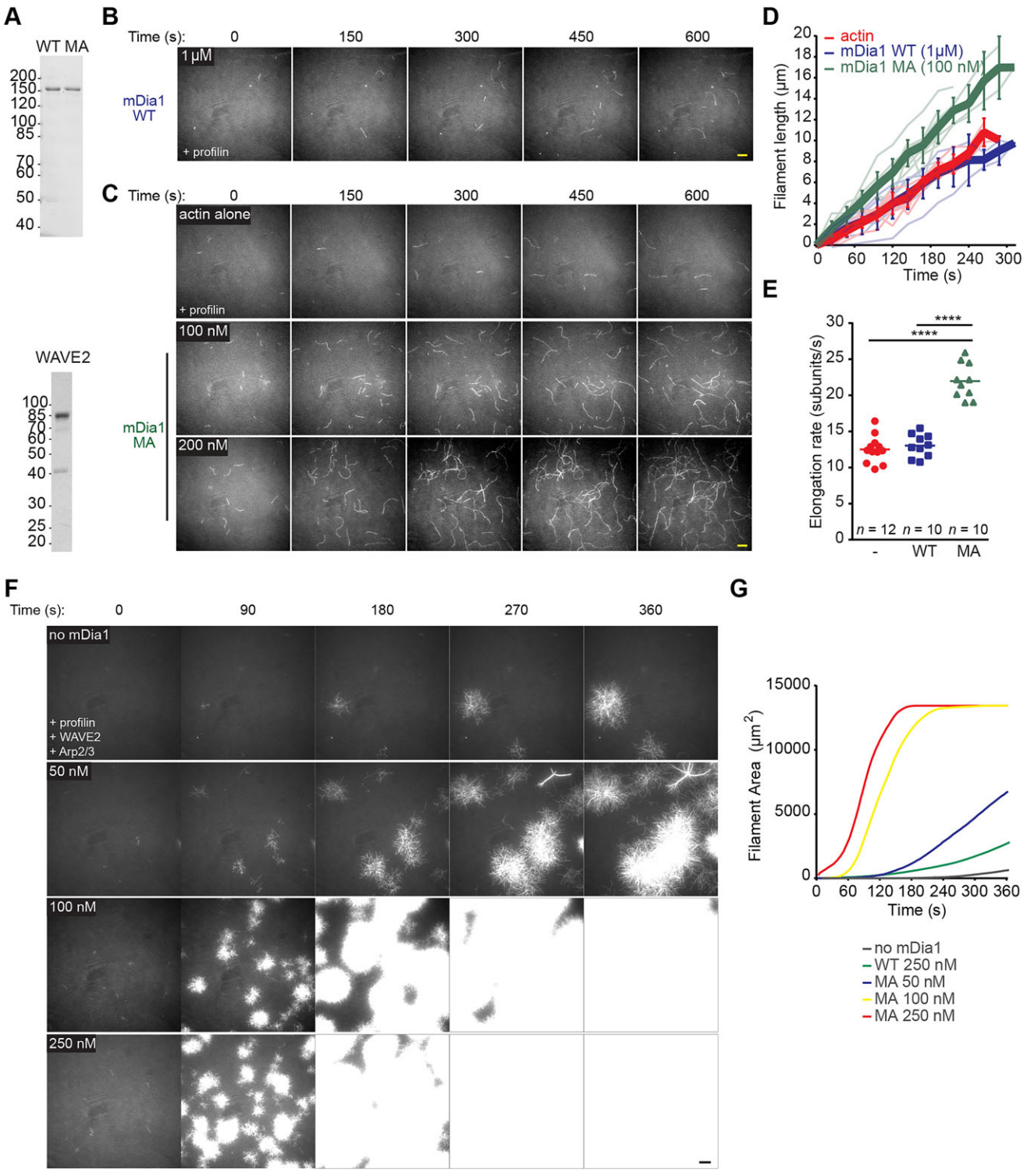

Fig. 4. Full-length mDia1 cooperates with the Arp2/3 complex to form branched actin networks. (A) Representative Coomassie gels showing purified recombinant wild-type (WT) and mutant (MA) mDia1 (1.5 µg) (top) and WAVE2 (2 µg) (bottom). (B–E) mDia1 promotes both nucleation and elongation of linear actin filaments in the presence of profilin-1 (profilin). (B,C) Representative frames extracted from TIRFm time-lapse imaging of actin polymerization at the indicated time and concentration of either mDia1 WT or its MA mutant. Profilin-bound actin (2.5 µM actin+5 µM profilin) was polymerized with the indicated concentration of mDia1 WT (B) or mDia1 MA (C). Scale bars: 10 µm. (D) At least ten filaments (thin lines) were tracked to determine filament length (mean±s.d., thick lines) versus time as described in the Materials and Methods. (E) Elongation rates were derived from D as described in the Materials and Methods. Scatter dot plots show average filament elongation rates. ****P<0.0001 (one-way ANOVA with Bonferroni's multiple comparison test; n=10–12 filaments). (F) mDia1 accelerates polymerization of branched actin filaments induced by the Arp2/3 complex. The Arp2/3 complex (20 nM) activated by WAVE2 (25 nM) was used to stimulate polymerization of profilin–actin (5 µM and 2.5 µM, respectively), either alone or with increasing concentrations of mDia1 MA. Representative frames extracted from TIRFm time-lapse movies illustrate actin polymerization at the indicated time (s) and concentration of mDia1 MA. Scale bar: 10 µm. (G) mDia1 cooperates with the Arp2/3 complex in making branched actin filaments. The area filled with filaments was quantified as described in the Materials and Methods. A representative dose–response experiment carried out on the same day is shown. A high-resolution version of this figure can be downloaded at http://dx.doi.org/10.6084/m9.figshare.1554814.

Journal of Cell Science (2015) 128, 3796-3810 doi:10.1242/jcs.176768

A

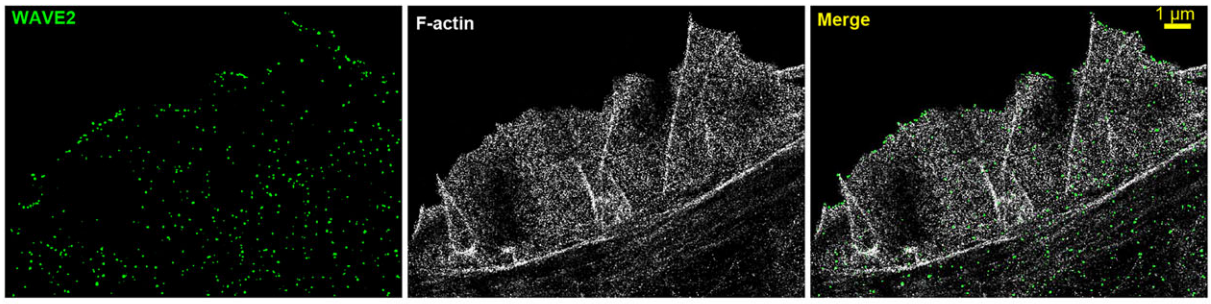

B

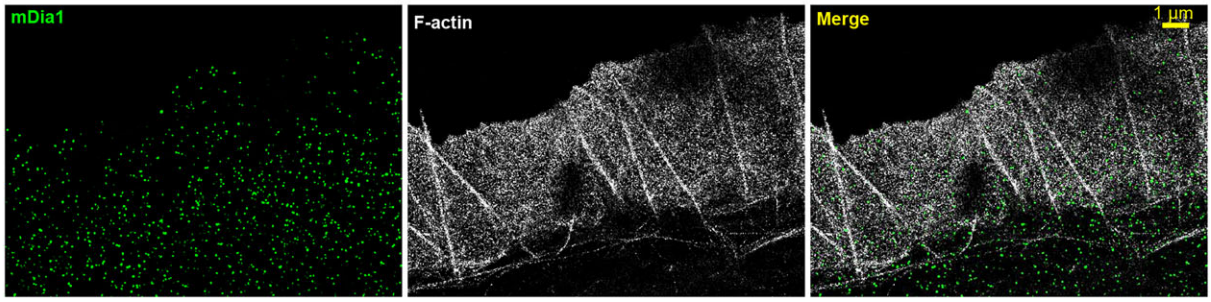

C

Protein	Distribution of the particles (%)			Relative density of the particles at the tip (%)	Relative abundance at the tip (a. u.)
	front	*middle*	*rear*		
mDia1 (*n* = 8 cells)	22.06 ± 2.00	30.88 ± 3.03	47.06 ± 3.14	4.41 ± 0.74	0.75 ± 0.11
WAVE2 (*n* = 7 cells)	45.67 ± 5.74 (***)	30.45 ± 5.44	28.51 ± 4.18 (**)	34.36 ± 9.21 (**)	6.45 ± 0.87 (****)

D

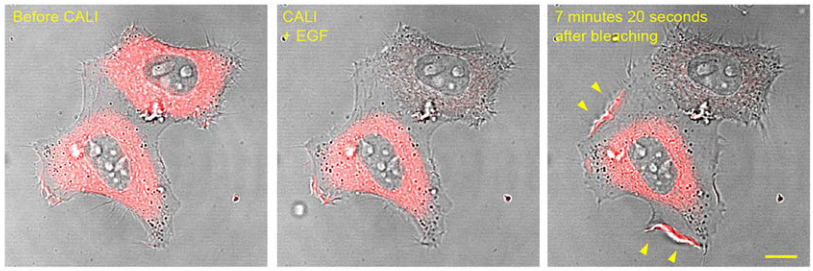

E

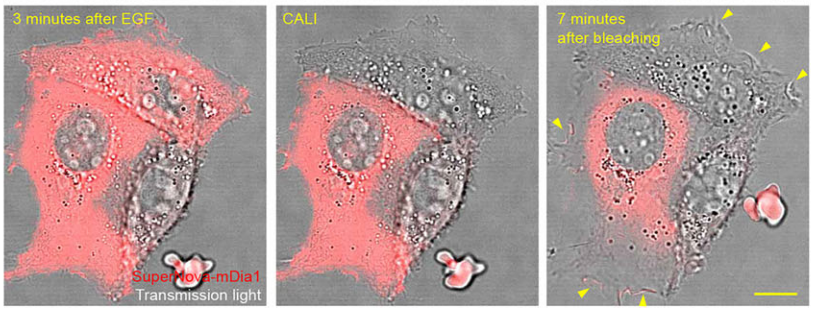

Fig. 5. mDia1 regulates initiation of lamellipodia and ruffles. (A,B) WAVE2 is enriched at the front of EGF-induced protrusions, whereas mDia1 populates the region behind the tip. HeLa cells were stimulated with EGF as in Fig. 1B, fixed and stained with Alexa-Fluor-647-labeled phalloidin (white in merge) and either anti-WAVE2 (A) or anti-mDia1 antibodies (B) (green in merge). Representative GSD SRm images are shown. The specificity of both antibodies was confirmed both by confocal and SRm (Figs S1A, S4E,F and data not shown, respectively). (C) Distribution of endogenous mDia1 and WAVE2 in lamellipodia and ruffles. Distribution, relative density and relative abundance were determined as indicated in the Materials and Methods. ***P*<0.01, ****P*<0.001, *****P*<0.0001 (one-way ANOVA was applied for the 'distribution'; and unpaired Student's *t*-test was used to calculate *P* values). Analyzed images were collected from three independent experiments (*n*=7–8 cells). (D) mDia1 is required for initiation of lamellipodia and ruffles. mDia1-knockdown #2 HeLa cells were transiently rescued with SuperNova–mDia1 and serum-starved overnight. CALI of SuperNova–mDia1 was performed prior to stimulation with EGF. Representative pre- and post-CALI frames extracted from Movie 6 show SuperNova–mDia1 (red) and phase-contrast images (gray). Yellow arrowheads highlight lamellipodia and ruffles. (E) mDia1 is dispensable for expansion of lamellipodia and ruffles. mDia1-knockdown #2 HeLa cells were transiently rescued with SuperNova–mDia1, serum starved overnight and then stimulated with EGF for 3 min prior to CALI. Representative pre- and post-CALI frames are taken from Movie 7 and depicted as in D. Scale bars: 10 µm. A high-resolution version of this figure can be downloaded at http://dx.doi.org/10.6084/m9.figshare.1554814.

Journal of Cell Science (2015) 128, 3796-3810 doi:10.1242/jcs.176768

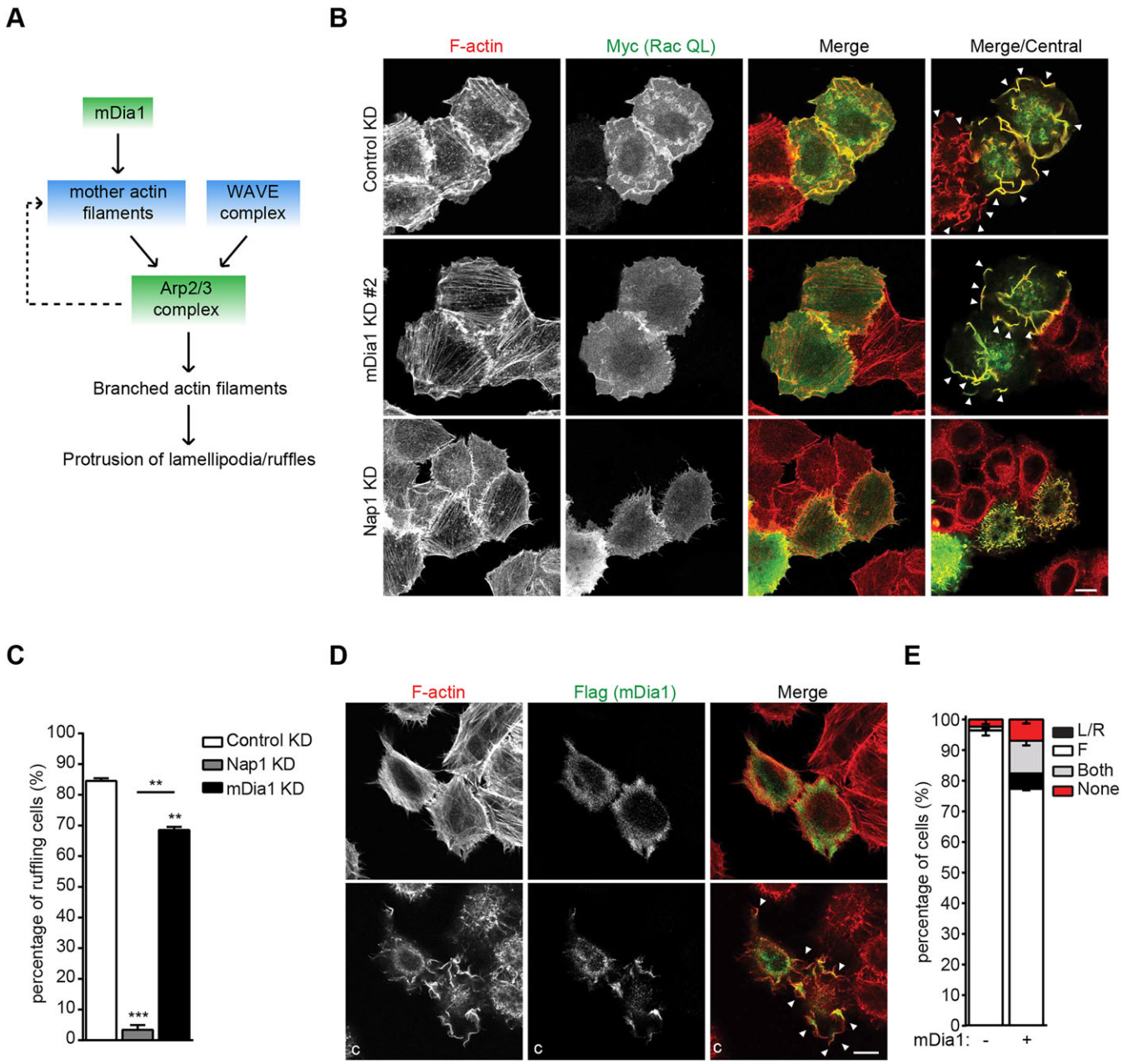

Fig. 6. mDia1 and the Arp2/3 complex cooperate to mediate efficient formation of lamellipodia and ruffles. (A) Schematic diagram showing that mDia1 polymerizes linear actin filaments that, together with the WAVE complex, are necessary for initial activation of the Arp2/3 complex and formation of lamellipodia and ruffles. Actin nucleators and Arp2/3 complex cofactors are boxed in green and light blue, respectively. Formation of branched actin filaments provides more mother actin filaments for the Arp2/3 complex and initiates a feed-forward loop making the contribution of mDia1 dispensable (dashed line). (B,C) Hyperactivation of the WAVE complex axis rescues ruffling in the mDia1-knockdown (KD) cells. (B) Myc-tagged RacQ61L (Myc-Rac QL) was overexpressed in control KD, mDia1 KD (#2) and Nap1 KD cells. After being serum starved, cells were fixed and stained with TRITC–phalloidin (red in merge) and anti-Myc antibodies (green in merge) to detect F-actin and Rac QL, respectively. Representative maximal projections and central confocal sections (Merge/Central) are shown. White arrowheads indicate ruffles. Scale bar: 10 µm. (C) The percentage of ruffling cells from B was quantified and plotted as mean±s.e.m. $^{**}P<0.01$ (one-way ANOVA with Bonferroni's multiple comparison test; $n\geq170$ cells from three independent experiments). (D,E) Hyperactivation of the mDia1 axis rescues EGF-induced ruffling in the Nap1 KD cells. (D) Flag-tagged mDia1 [Flag (mDia1)] was overexpressed in Nap1-knockdown cells and imaged using confocal microscopy. Representative maximal projections and central sections (c) are shown. White arrowheads mark ruffles. Scale bar: 10 µm. (E) Percentage of cells from D showing the indicated EGF-induced protrusions (L/R, lamellipodia and ruffles; F, filopodia) was quantified and plotted as mean±s.e.m. ($n\geq159$ cells from three independent experiments, Table S6). A high-resolution version of this figure can be downloaded at http://dx.doi.org/10.6084/m9.figshare.1554814.

(Insall and Machesky, 2009), movement of MDA-MB-231 cells was reduced by knockdown of mDia1 or pharmacological inhibition of the Arp2/3 complex (Nolen et al., 2009) (Fig. 7D). Of note, concomitant decrease of mDia1 expression and Arp2/3 complex activity had additional negative effects on the migratory abilities of MDA-MB-231 cells (Fig. 7D). This observation is consistent with the Arp2/3 complex having also mDia1-independent functions that, together with membrane protrusions, allow for optimal cell migration. As cell directionality was not affected by any of these perturbations (Fig. 7E), these results collectively suggest that mDia1 and the Arp2/3 complex specifically support actin-based protrusion of the plasma membrane for cell motility.

Journal of Cell Science (2015) 128, 3796-3810 doi:10.1242/jcs.176768

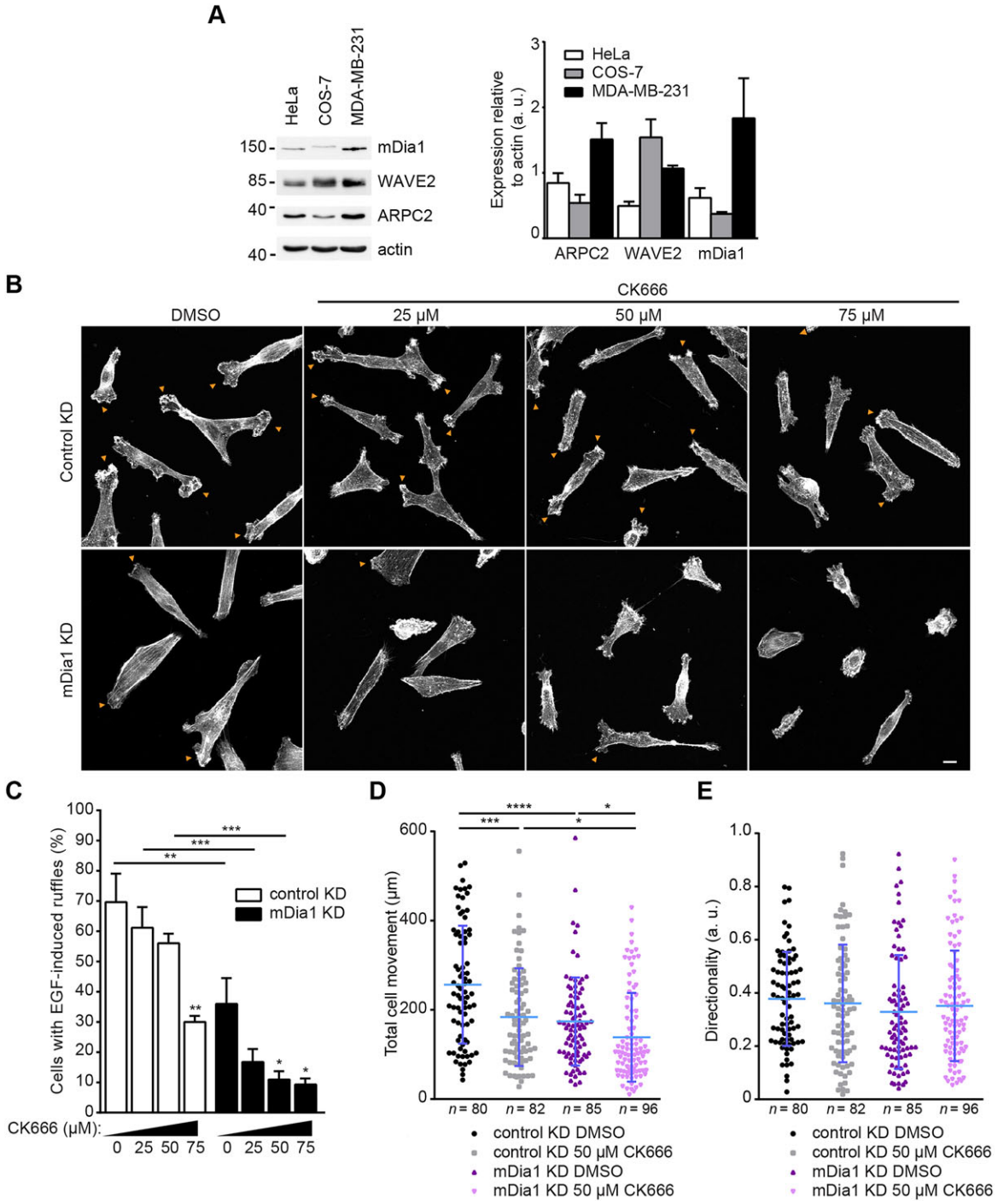

Fig. 7. Expression and activity of mDia1 and the Arp2/3 complex determine the contribution of either nucleator to ruffling and cell migration. (A) mDia1, WAVE2 and Arp2/3 attain different expression levels in HeLa, COS-7 and MDA-MB-231 cells. Left, total cell lysates (30 µg) were compared using the indicated antibodies. One of three experiments that were performed with similar results is shown. Right, bar graph depicting densitometric quantification of ARPC2, mDia1 and WAVE2 normalized with respect to actin levels, as obtained from three independent experiments [Expression relative to actin (a.u.), mean±s.e.m.]. (B,C) EGF-induced ruffling requires mDia1 upon attenuation of Arp2/3 complex activity. (B) Control and mDia1-knockdown (KD) MDA-MB-231 cells were plated on collagen-coated coverslips and were serum starved overnight. Cells were incubated with increasing concentrations of the Arp2/3 complex inhibitor CK666 or DMSO for 30 min and then stimulated with EGF (25 ng ml^{-1}) for 7 min. After fixation, cells were stained with TRITC–phalloidin. Representative maximal projections are shown. Orange arrowheads mark ruffles. Scale bar: 10 µm. (C) The percentage of ruffling cells from the experiments in B was quantified and plotted as mean±s.d. *P<0.05; **P<0.01; ***P<0.001 (one-way ANOVA with Bonferroni's multiple comparison test; n≥200 cells from two independent experiments). (D,E) mDia1 and the Arp2/3 complex cooperate to promote cell migration. Control and mDia1 KD MDA-MB-231 cells were plated on collagen-coated chambers and serum-starved overnight. The next day, cells were exposed to either DMSO or CK666 (50 µM) for 45–60 min during formation of the EGF gradient and then imaged. Scatter dot plots show the mean±s.d. of total cell movement (D) and directionality (E). *P<0.05; ***P<0.001; ****P<0.0001 (one-way ANOVA with Bonferroni's multiple comparison test; n=80–96 cells from two independent experiments). A high-resolution version of this figure can be downloaded at http://dx.doi.org/10.6084/m9.figshare.1554814.

Journal of Cell Science (2015) 128, 3796-3810 doi:10.1242/jcs.176768

DISCUSSION

In this study, we show that the actin nucleator mDia1 acts in concert with the Arp2/3 complex to promote initiation of lamellipodia and ruffles. At the mechanistic level, we demonstrate that mDia1 polymerizes linear actin filaments allowing the Arp2/3 complex to set in motion auto-catalytic assembly of branched actin filaments. These findings highlight that the lamellipodium- and ruffle-initiating machinery consists of two actin nucleators that act sequentially. On this ground, we propose that both the WAVE complex and the polymerization of mother actin filaments undergo regulation within nascent lamellipodia and ruffles. As mDia1 did not bind either the WAVE complex or the Arp2/3 complex, our data are consistent with a model in which EGFR activation recruits and activates mDia1 at the plasma membrane through Rho, thereby leading to the formation of new linear actin filaments (Fig. 8). Rac-induced activation of the WAVE complex at the plasma membrane cooperates with the actin filaments generated by mDia1 in promoting initial activation of the Arp2/3 complex. After the initiation phase, auto-catalytic nucleation of branched actin filaments by the Arp2/3 complex is sufficient to support the expansion of lamellipodia and ruffles (Fig. 8).

The mechanism regulating the initiation of lamellipodia and ruffles fills a huge gap in our understanding of these actin-based protrusions, as explained below. Pioneering biochemical and molecular genetic studies discovered that pre-existing mother actin filaments and the NPF WAVE are required for activation of the Arp2/3 complex, ensuing nucleation of branched actin filaments and formation of lamellipodia and ruffles. As filamentous actin is an essential cofactor in the Arp2/3-complex activation mechanism, actin polymerization by the Arp2/3 complex is an auto-catalytic reaction using newly assembled branched actin filaments as a template for further rounds of branching (Beli et al., 2008; Goley and Welch, 2006; Innocenti et al., 2004; Le Clainche and Carlier, 2008; Pollard, 2007; Pollard and Borisy, 2003; Rotty et al., 2013; Suraneni et al., 2012; Yamazaki et al., 2003; Yan et al., 2003). Although these seminal studies have illuminated the mechanism that sustains expansion of lamellipodia and ruffles, the initiation thereof has remained so far enigmatic because the origin and availability of the pre-existing actin filaments mediating initial activation of the Arp2/3 complex were mysterious. In fact, both aged and tropomyosin-bound actin filaments serve as very poor mother filaments for the Arp2/3 complex (Blanchoin et al., 2000, 2001; Bugyi and Carlier, 2010; DesMarais et al., 2002; Iwasa and Mullins, 2007). Furthermore, the actin cortex is enriched in myosins and other actin-binding proteins that prevent binding of the Arp2/3 complex to actin filaments (Biro et al., 2013). Conversely, *de novo* polymerized actin filaments can be efficiently used as mother filaments by the Arp2/3 complex (Blanchoin et al., 2000; Bugyi and Carlier, 2010). Thus, the initiation of lamellipodia and ruffles raises the paradox that for the Arp2/3 complex to make branched actin filaments it requires prior polymerization of new actin filaments. Two possible solutions to this paradox have been proposed: (1) cofilin-mediated severing might create free barbed ends and polymerizing actin filaments that can activate the Arp2/3 complex (Ichetovkin et al., 2002), and (2) SPIN90 (also known as NCKIPSD)-mediated activation of the Arp2/3 complex without pre-existing actin filaments (Wagner et al., 2013). However, neither mechanism seems to be satisfactory as knockdown and CALI of cofilin results in enlargement of lamellipodia and ruffles and increased F-actin levels in cells employing the mesenchymal mode of migration (Hotulainen et al., 2005; Rogers et al., 2003; Sidani et al., 2007; Vitriol et al., 2013), and full-length SPIN90 does not activate the Arp2/3 complex (Fukuoka et al., 2001 and data not shown). In this regard, the involvement of another actin nucleator in the mechanism regulating initial activation of the Arp2/3 complex would resolve this paradox.

The ability of mDia1 to polymerize linear actin filaments for the Arp2/3 complex solves the mystery of the pre-existing mother filaments thereby unveiling the mechanism regulating the initiation of lamellipodia and ruffles. Remarkably, this mechanism also provides an explanation for the puzzling and neglected observations that dendritic and T cells obtained from mDia1-knockout mice cannot form lamellipodia or ruffles, and exhibit defective cell motility (Sakata et al., 2007; Tanizaki et al., 2010).

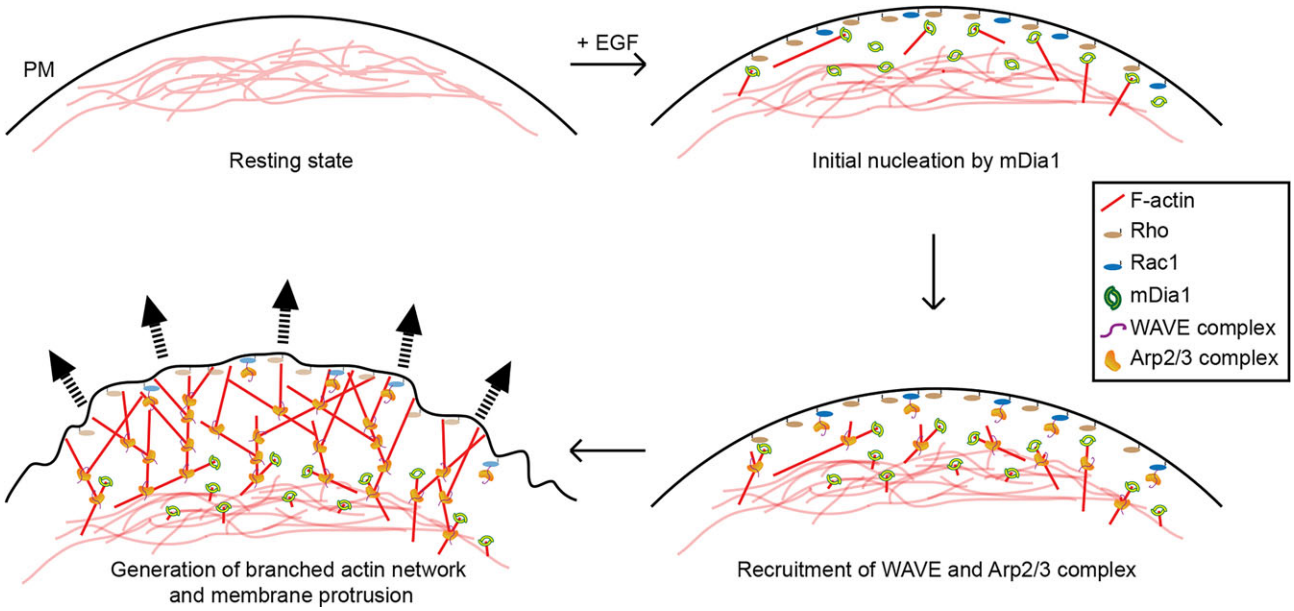

Fig. 8. Working model for the cooperation between mDia1 and Arp2/3 in the making of lamellipodia and ruffles. Working model for the cooperation between mDia1 and Arp2/3 in the making of lamellipodia and ruffles. PM, plasma membrane; thick black arrows indicate protrusion.

Journal of Cell Science (2015) 128, 3796-3810 doi:10.1242/jcs.176768

Our findings reinforce the notion that formin family proteins are tightly intertwined with the biogenesis of lamellipodia and ruffles. Interestingly, it appears that different formins regulate specific phases of the life cycle of lamellipodia and ruffles: we show that mDia1 exerts a unique role in the initiation phase, whereas FMNL2, mDia2, mDia1 and other formins might have partially redundant roles during the expansion phase (Block et al., 2012; Gupton et al., 2007).

Remarkably, the role of mDia1 in initiating Arp2/3-complex-dependent actin polymerization might extend beyond the protrusion of lamellipodia and ruffles, and cell migration. In fact, recent indirect evidence suggests that mDia1 might act upstream of the Arp2/3 complex in nucleating cortical actin during mitosis (Bovellan et al., 2014). However, the cooperation between mDia1 and the Arp2/3 complex in the assembly of the cortical actin cytoskeleton is cell cycle dependent, as interphase cells have a cortex composed of independent mDia1- and Arp2/3-complex-nucleated actin networks (Bovellan et al., 2014).

As NPFs and mother filaments are obligatory cofactors of the Arp2/3 complex, we speculate that cooperation between dedicated NPFs, and actin nucleators producing mother filaments might be a general mechanism to control the execution of Arp2/3-complex-dependent processes at specific locations within the cell (Goley and Welch, 2006; Rotty et al., 2013).

In conclusion, the cooperation between mDia1 and the Arp2/3 complex in the making of lamellipodia and ruffles enables cells to sense and integrate different signals regulating membrane protrusion and mesenchymal cell migration. Given that lamellipodia and ruffles are key to a variety of developmental and homeostatic processes linked to a growing number of diseases, including cancer (Goley and Welch, 2006; Machesky, 2008), the mechanism regulating the initiation of lamellipodia and ruffles has a paramount importance in both biology and medicine.

MATERIALS AND METHODS

Chemicals and reagents

High-glucose Dulbecco's modified Eagle's medium (DMEM) supplemented with pyruvate and stable glutamine was from PAA. Protease inhibitor EDTA-free cocktail and X-tremeGene9 were from Roche. Human recombinant EGF (AF-100-15) was from Tebu-Bio. If not otherwise specified, all other chemicals were from Sigma-Aldrich.

Antibodies

Antibodies were as follows: mouse anti-β-actin (AC-15), mouse anti-tubulin and anti-Flag M2 (Sigma-Aldrich), mouse anti-mDia1, mouse anti-p21 ARPC3, mouse anti-Rac1 and mouse anti-Rho (BD Transduction Laboratories), rabbit anti-WAVE1 (Cell Signaling), mouse anti-fascin (MAB3582, Chemicon), mouse anti-Myc (clone 9E10; Babco), mouse anti-mDia1 (D3, Santa Cruz Biotechnology), goat anti-p34 ARPC2 (Imgenex), rabbit anti-mDia3 (Bethyl Laboratories), rabbit polyclonal anti-KillerRed (Evrogen), rabbit anti-EGFR and rabbit anti-Nap1 (Innocenti et al., 2005), and rabbit anti-mDia2 (Isogai et al., 2015a,b) antibodies. Mouse anti-WAVE2 antibodies were generated in house and characterized in Fig. S4E,F. Horseradish peroxidase (HRP)-conjugated antibodies were from Bio-Rad. Alexa-Fluor-488- and Alexa-Fluor-561-conjugated antibodies were from Invitrogen.

Expression vectors

pGEX-C21 and Flag-tagged full-length mDia1 were a kind gift from John Collard (Cell Biology, Netherlands Cancer Institute, The Netherlands) and Wouter Moolenaar (Cell Biology, Netherlands Cancer Institute, The Netherlands), respectively. pEGFP-C was from ClonTech. SuperNova/pCDNA3 was from Takeharu Nagai (Research Institute of Electronic Sciences, Hokkaido University, Japan). pRK-Rac1-myc Q61L, pCDNA3-Flag-mDia2 and pCDNA3-Flag-Mena were previously described (Beli et al., 2008). Human profilin-1 was amplified by PCR, cloned in the bacterial and mammalian expression vectors pGEX-6P1 and pEGFP-C1, respectively, and sequence verified. mDia1 constructs harboring either point mutations [mDia1 V160D and mDia1 M1182A (MA)] or deletion of the FH2 domain (amino acids 752–1174; mDia1ΔFH2) were generated by PCR using Phusion Hot-Start II High-Fidelity DNA polymerase (Thermo Scientific). pSuperNova-mDia1 (SN–mDia1) was derived from pEGFP-mDia1 by swapping EGFP with SuperNova and was sequence-verified. Primers are listed in Table S10.

Protein purification and biochemical assays

Full-length Flag-tagged mDia1 and WAVE2 proteins were purified as the PIR121–Nap1 subcomplex (Innocenti et al., 2004). Proteins were flash-frozen in storage buffer (50 mM Tris-HCl pH 7.6, 150 mM NaCl, 10% glycerol and 1 mM DTT) and kept at −80°C.

GST–RBD (Rhotekin) and GST–CRIB (PAK) were purified as previously described (Innocenti et al., 2004). Human profilin-1 was isolated from bacteria as a GST fusion protein and then cleaved with PreScission protease (GE Healthcare) as previously described (Galovic et al., 2011).

RBD and CRIB pulldown assays were carried out by incubating 500 µg of total cell lysates with 30 µg of GST–RBD and GST–CRIB, respectively, as previously described (Innocenti et al., 2004).

Arp2/3 protein complex (#RP01-A) and Atto488-labeled actin (#8153-02) were purchased from Cytoskeleton and Hypermol, respectively.

Cell culture, transfections and generation of stable knockdown cell lines

293T, HeLa, COS-7 and MDA-MB-231 cells were cultured in DMEM supplemented with 10% heat-inactivated fetal calf serum (FCS). 293T cells were transfected using a standard calcium phosphate protocol. HeLa cells were transfected with X-tremeGene 9 (Roche) according to the manufacturer's instructions. Stable mDia1-knockdown HeLa, COS-7 and MDA-MB-231 cells were obtained by lentiviral infection using the MISSION® TRC shRNA TRCN0000118678 (shmDia1 #1) and TRCN0000118677 (shmDia1 #2), and subsequent selection with puromycin (Invitrogen). Stable mDia3-knockdown in COS-7 cells was obtained by lentiviral infection using the MISSION® TRC shRNA TRCN0000083891 and subsequent selection with puromycin (Invitrogen). Nap1-knockdown cells were as previously described (Beli et al., 2008).

Barbed ends assay

Control and mDia1-knockdown #2 cells were seeded on gelatin-coated coverslips and serum starved overnight. Cells were either left untreated or stimulated with EGF for 40 and 100 s prior to barbed-end labeling. Barbed ends were labeled by incubating cells with 0.5 µM Atto488-labeled G-actin in permeabilization buffer (138 mM KCl, 4 mM $MgCl_2$, 10 mM PIPES pH 6.8, 3 mM EGTA, 0.025% saponin, 1% BSA and 1 mM fresh ATP) for 1 min. Cells were briefly washed with permeabilization buffer, fixed with 4% paraformaldehyde in PIPES buffer (80 mM PIPES pH 6.8, 5 mM EGTA, 2 mM $MgCl_2$) and processed for immunofluorescence. Total free barbed ends were determined by measuring the total intensity of Atto488-labeled G-actin per image, and normalized to the total cell area (normalized intensity per area).

Confocal and super-resolution microscopy

HeLa cells, COS-7 cells and MDA-MB-231 cells were seeded on gelatin-coated, fibronectin-coated and collagen-I-coated coverslips, respectively. Cells were serum starved overnight and either left untreated or stimulated with EGF (100 ng ml^{-1} unless otherwise stated) for 7 min or as indicated. Cells were fixed, permeabilized and stained as previously described (Isogai et al., 2015b). Images were acquired sequentially on a CLSM Leica TCS SP5 as previously described (Isogai et al., 2015b).

CALI was performed on mDia1-knockdown HeLa cells transiently transfected with SuperNova–mDia1 and serum starved overnight. Live-cell confocal images were acquired on a CLSM Leica TCS SP5 microscope equipped with a humidified climate chamber with 5% CO_2 at 37°C. CALI was obtained exposing SuperNova–mDia1-expressing cells to intense laser light (100% laser power, 561 nm).

For ground state depletion (GSD) super-resolution microscopy, cells were stimulated for 3 min with EGF and fixed as above. Fixed samples were treated with freshly prepared 0.1% $NaBH_4$ in PBS for 7 min. Samples were extensively washed with PBS and blocked with 5% BSA for 30 min at room temperature, stained with the primary antibodies followed by the secondary antibodies and phalloidin (Invitrogen). Imaging was carried out on a Leica SR-GSD microscope. Images were taken in EPI mode at 100 frames per second and 10,000–15,000 frames were collected (total measurement time of ∼5 min). Images were taken sequentially in decreasing excitation and emission wavelength order in the presence of an oxygen scavenging system [10% glucose, 0.5 mg/ml glucose oxidase, 40 µg/ml catalase and 50 mM cysteamine (MEA)].

Measurement of protein enrichment at the cell edge

HeLa cells seeded on gelatin-coated coverslips were transfected with EGFP and serum starved overnight. Cells were either left untreated or stimulated with EGF (100 ng ml^{-1}) for the indicated time. Cells were fixed, stained and imaged as above. The relative abundance of EGFP and mDia1 at the edges were assessed by calculating the relative intensity of either protein at the cell edge over the mean intensity in the cytoplasm (ratio; arbitrary units). EGFP served as a volumetric marker and relative enrichment of mDia1 at the cell edge was determined by normalizing against EGFP (normalized relative intensity; arbitrary units).

Ratiometric measurement of Rho GTPase activities by fluorescence resonance energy transfer

Cells were seeded on gelatin-coated coverslips, and transiently transfected with Rac1 or RhoA fluorescence resonance energy transfer (FRET)-based biosensors [dimerization-optimized reporters for activation of Rho GTPases 'DORA,' which are an improved version of Raichu (Itoh et al., 2002) and RhoA sensors (Pertz et al., 2006)]. Cells were serum starved overnight prior to the experiment. Experiments were performed in DMEM-F12 medium without Phenol Red (Invitrogen), in a humidified chamber with 5% CO_2 at 37°C. Images were taken on a Leica TCS SP5 confocal equipped with an oil-immersion HCX PL APO CS 63.0× (NA 1.40) 'Lambda-Blue' objective and LAS-AF acquisition software extended with MatrixScreener (Leica Microsystems). Fluorophores were excited with 458 nm laser light and two images (emission range from 465–510 nm and 520–600 nm) were acquired simultaneously. The laser power was set at a level that prevented fluorophore saturation, and neither photobleaching nor phototoxic effects were observed. Four fields of view were followed within a single experiment with a time lapse of 20–25 s between individual images [data were linearly interpolated (SciPy, Oliphant 2007) to 25-s intervals]. Rho GTPase activity is presented as a ratio between YFP and CFP channels, set at 1 at the onset of the experiment.

Quantification of the distribution of WAVE2 and mDia1 within EGF-induced protrusions

Ruffles and lamellipodia were segmented in three equal areas denoted as front, middle and rear, with the front area being the distal part relative to the cell body. Knowing the physical size of a pixel, the total area (μm^2) of both the entire protrusion and each segment thereof were obtained from phalloidin images. WAVE2 or mDia1-positive particles in the total area (or in each segment) were quantified with ImageJ using the 'Analyze particles' function after supervised segmentation. The distribution of WAVE2 and mDia1 was then calculated as number of particles in a given segment divided over the total number of particles within the entire protrusion (expressed as a percentage).

For the quantification of particles at the ruffle and lamellipodium tip, the area and particle count were restricted to 5 pixels width (0.1 µm) from the edge, as determined using phalloidin staining. WAVE2- or mDia1-positive particles at the tip and in the remaining part of the protrusion were quantified with the ImageJ using the 'Analyze particles' function after supervised segmentation. The relative density of WAVE2 and mDia1 at the tip (expressed as percentage) was calculated as number of particles at the tip divided over the total number of particles within the entire protrusion. The relative abundance of WAVE2 and mDia1 at the tip (expressed as a ratio; arbitrary units) was calculated by dividing the density of WAVE2 or mDia1 at the tips (particles/μm^2) over the average density of WAVE2 or mDia1 (particles/μm^2) within the entire protrusion.

Classification of EGF-induced protrusions

Ruffles and filopodia were classified as previously described (Beli et al., 2008). Cellular protrusions were scored manually and grouped in following three categories: (1) ruffles and lamellipodia when filopodia were absent, (2) filopodia when ruffles and lamellipodia were absent, (3) both when these different actin-based protrusions coexisted in the same cell, and (4) none when protrusions were absent. The origin of the protrusive organelles was verified using bona fide molecular markers of lamellipodia, ruffles and filopodia (Fig. S1). At least 50–100 cells were counted per condition per experiment and data are shown as mean±s.e.m. from three independent experiments unless otherwise indicated.

TIRFm-based actin polymerization assays

Glass coverslips (24×50 mm, #1.5) were washed for 30 min in acetone, 10 min in absolute ethanol, rinsed in double-distilled water (ddH_2O), and cleaned for 2 h in 2% Helmanex. Cleaned coverslips were rinsed extensively with ddH_2O, and dried with compressed air flow.

Coverslips were derivatized by coating with 1 mg/ml mPEG-silane MW 5000 (Laysan Bio, Arab, AL) in 96% ethanol for 18 h at room temperature with gentle shaking. Next, coverslips were rinsed extensively with absolute ethanol and ddH_2O, dried using a compressed air flow and stored for up to 1 week.

Flow cells were assembled by placing four parallel strips of double-sided tape (15 mm×2 mm×70 µm) onto a cleaned glass slide (25×75 mm) with ∼15 mm spacing between the strips. A polyethylene glycol (PEG)-coated coverslip was then positioned over the strips to obtain three separate flow chambers.

TIRFm was performed using a Leica DMI600B inverted microscope (Leica Microsystems GmbH, Germany) equipped with a Multi-Color laserbox with four diode lasers (405, 488, 561 and 635 nm) and AOTF control, a PLAN APO 63×/1.47 Oil HCX TIRF objective, and an air-cooled Hamamatsu 9100-02 EMCCD High Speed camera with a pixel size of 8 μm^2. Focus was maintained by the built-in adaptive focus control (AFC) unit.

Actin polymerization was carried out in TIRF buffer [10 mM Tris-HCl pH 7.6, 100 mM KCl, 1 mM $MgCl_2$, 0.2 mM EGTA, 0.2 mM ATP, 0.5 mM DTT, 15 mM glucose, 20 µg/ml catalase, 100 µg/ml glucose oxidase, 1% BSA and 0.5% methylcellulose (4000 cP)]. Actin regulatory proteins were diluted into TIRF buffer, then rapidly mixed with G-actin (20% Atto488-labeled G-actin) and introduced into the flow cell. The time between initial mixing and the start of TIRFm recording was typically 15–20 s. Images were acquired every 3 s. Final protein concentrations were as follows: 2.5 µM actin, 5 µM profilin-1, 25 nM WAVE2 and 20 nM of the Arp2/3 complex. Concentrations of mDia1 are depicted in the figures. The final amount of glycerol never exceeded 1%. Single filaments were manually tracked in ImageJ. Elongation rate (subunits/s) was calculated considering that 1 µm of F-actin corresponds to 370 monomers. All experiments are representative of at least two independent protein preparations assayed with similar outcome. Filament area was determined using the ImageJ plugin 'Area Calculator'. Lines in the graphs represent connected points.

Migration assays

Approximately 15,000–18,000 control knockdown and mDia1-knockdown MDA-MB-231 cells were plated on collagen-coated µ-Slide Chemotaxis units and serum starved overnight. Cells were then incubated with CK666 (50 µM) or control DMSO for 45–60 min while a gradient of EGF was forming (final concentration of 25 ng ml^{-1}). Next, cells were imaged every 2 min on a Zeiss Axio Observer Z1 microscope (Carl Zeiss) equipped with a LD Plan-Neofluar Ph2 20× (NA 0.40) objective, operated with Zeiss Microscope Software ZEN 2012. Individual cells were tracked using the 'Manual Tracking' plugin for ImageJ. Average total cell movement and directionality were computed using the 'Chemotaxis Tool' plugin for ImageJ (www.ibidi.com). At least 40 cells per condition were tracked in two independent experiments.

Total RNA isolation and qRT-PCR analyses

Total RNA and complementary DNA (cDNA) were obtained as previously described (Isogai et al., 2015a,b). Quantitative real-time PCR (qRT-PCR) reactions were set up using 5–10 ng of cDNA as a template and gene-specific primers (200 nM, Isogai et al., 2015b) in a StepOnePlus Real-Time PCR system (Applied Biosystems). All reactions produced single amplicons (100–200 bps), which allowed us to equate one threshold cycle difference. Results were normalized with respect to *GAPDH* expression. mRNA levels were quantified according to the $2^{-\Delta\Delta Ct}$ method (Ct, cycle threshold). Genes with Ct values of ≥31 were considered as not expressed.

Statistics

Statistical analyses were performed using GraphPad Prism version 6.01 (GraphPad Software, San Diego, CA, USA, www.graphpad.com). In all cases: *P<0.05; **P<0.01; ***P<0.001; ****P<0.0001.

Acknowledgements

We thank J. Collard, W. Moolenaar and T. Nagai for reagents, L. Omen and L. Brocks from the NKI Microscopy Facility for technical assistance and E. Argenzio for critically reading the manuscript.

Competing interests

The authors declare no competing or financial interests.

Author contributions

T.I. generated and characterized knockdown cell lines, purified proteins, imaged TIRFm-based actin polymerization, performed rescue experiments, barbed-end assays, volumetric analysis and migration assays and analyzed data. D.L.-P. acquired and analyzed GSD super-resolution images. K.M.K. imaged FRET experiments and quantified data. R.v.d.K. generated anti-WAVE2 antibodies and provided technical support. M.I. performed pull-down experiments, purified proteins and analyzed data. K.J. supervised GSD analyses. T.I. and M.I. conceived the project and designed the experiments. M.I. coordinated the work and wrote the manuscript.

Funding

This study was supported by a grant from Stichting Technische Wetenschappen [grant number 12150] to K.J.; and a junior group grant from the Cancer Genomics Centre [CGC 2009-2013 to M.I.].

Supplementary information

Supplementary information available online at
http://jcs.biologists.org/lookup/suppl/doi:10.1242/jcs.176768/-/DC1

References

Alberts, A. S. (2001). Identification of a carboxyl-terminal diaphanous-related formin homology protein autoregulatory domain. *J. Biol. Chem.* **276**, 2824-2830.

Bear, J. E. and Gertler, F. B. (2009). Ena/VASP: towards resolving a pointed controversy at the barbed end. *J. Cell Sci.* **122**, 1947-1953.

Beli, P., Mascheroni, D., Xu, D. and Innocenti, M. (2008). WAVE and Arp2/3 jointly inhibit filopodium formation by entering into a complex with mDia2. *Nat. Cell Biol.* **10**, 849-857.

Biro, M., Romeo, Y., Kroschwald, S., Bovellan, M., Boden, A., Tcherkezian, J., Roux, P. P., Charras, G. and Paluch, E. K. (2013). Cell cortex composition and homeostasis resolved by integrating proteomics and quantitative imaging. *Cytoskeleton* **70**, 741-754.

Blanchoin, L., Amann, K. J., Higgs, H. N., Marchand, J. B., Kaiser, D. A. and Pollard, T. D. (2000). Direct observation of dendritic actin filament networks nucleated by Arp2/3 complex and WASP/Scar proteins. *Nature* **404**, 1007-1011.

Blanchoin, L., Pollard, T. D. and Hitchcock-DeGregori, S. E. (2001). Inhibition of the Arp2/3 complex-nucleated actin polymerization and branch formation by tropomyosin. *Curr. Biol.* **11**, 1300-1304.

Block, J., Breitsprecher, D., Kuhn, S., Winterhoff, M., Kage, F., Geffers, R., Duwe, P., Rohn, J. L., Baum, B., Brakebusch, C. et al. (2012). FMNL2 drives actin-based protrusion and migration downstream of Cdc42. *Curr. Biol.* **22**, 1005-1012.

Bovellan, M., Romeo, Y., Biro, M., Boden, A., Chugh, P., Yonis, A., Vaghela, M., Fritzsche, M., Moulding, D., Thorogate, R. et al. (2014). Cellular control of cortical actin nucleation. *Curr. Biol.* **24**, 1628-1635.

Brandt, D. T., Marion, S., Griffiths, G., Watanabe, T., Kaibuchi, K. and Grosse, R. (2007). Dia1 and IQGAP1 interact in cell migration and phagocytic cup formation. *J. Cell Biol.* **178**, 193-200.

Bugyi, B. and Carlier, M.-F. (2010). Control of actin filament treadmilling in cell motility. *Annu. Rev. Biophys.* **39**, 449-470.

Chan, K. T., Creed, S. J. and Bear, J. E. (2011). Unraveling the enigma: progress towards understanding the coronin family of actin regulators. *Trends Cell Biol.* **21**, 481-488.

Chesarone, M. A., DuPage, A. G. and Goode, B. L. (2010). Unleashing formins to remodel the actin and microtubule cytoskeletons. *Nat. Rev. Mol. Cell Biol.* **11**, 62-74.

Colucci-Guyon, E., Niedergang, F., Wallar, B. J., Peng, J., Alberts, A. S. and Chavrier, P. (2005). A role for mammalian diaphanous-related formins in complement receptor (CR3)-mediated phagocytosis in macrophages. *Curr. Biol.* **15**, 2007-2012.

Dang, I., Gorelik, R., Sousa-Blin, C., Derivery, E., Guerin, C., Linkner, J., Nemethova, M., Dumortier, J. G., Giger, F. A., Chipysheva, T. A. et al. (2013). Inhibitory signalling to the Arp2/3 complex steers cell migration. *Nature* **503**, 281-284.

DesMarais, V., Ichetovkin, I., Condeelis, J. and Hitchcock-DeGregori, S. E. (2002). Spatial regulation of actin dynamics: a tropomyosin-free, actin-rich compartment at the leading edge. *J. Cell Sci.* **115**, 4649-4660.

Fukuoka, M., Suetsugu, S., Miki, H., Fukami, K., Endo, T. and Takenawa, T. (2001). A novel neural Wiskott-Aldrich syndrome protein (N-WASP) binding protein, WISH, induces Arp2/3 complex activation independent of Cdc42. *J. Cell Biol.* **152**, 471-482.

Galovic, M., Xu, D., Areces, L. B., van der Kammen, R. and Innocenti, M. (2011). Interplay between N-WASP and CK2 optimizes clathrin-mediated endocytosis of EGFR. *J. Cell Sci.* **124**, 2001-2012.

Gautreau, A., Ho, H.-Y., Li, J., Steen, H., Gygi, S. P. and Kirschner, M. W. (2004). Purification and architecture of the ubiquitous Wave complex. *Proc. Natl. Acad. Sci. USA* **101**, 4379-4383.

Goh, W. I., Sudhaharan, T., Lim, K. B., Sem, K. P., Lau, C. L. and Ahmed, S. (2011). Rif-mDia1 interaction is involved in filopodium formation independent of Cdc42 and Rac effectors. *J. Biol. Chem.* **286**, 13681-13694.

Goley, E. D. and Welch, M. D. (2006). The ARP2/3 complex: an actin nucleator comes of age. *Nat. Rev. Mol. Cell Biol.* **7**, 713-726.

Gould, C. J., Maiti, S., Michelot, A., Graziano, B. R., Blanchoin, L. and Goode, B. L. (2011). The formin DAD domain plays dual roles in autoinhibition and actin nucleation. *Curr. Biol.* **21**, 384-390.

Gupton, S. L., Eisenmann, K., Alberts, A. S. and Waterman-Storer, C. M. (2007). mDia2 regulates actin and focal adhesion dynamics and organization in the lamella for efficient epithelial cell migration. *J. Cell Sci.* **120**, 3475-3487.

Hotulainen, P., Paunola, E., Vartiainen, M. K. and Lappalainen, P. (2005). Actin-depolymerizing factor and cofilin-1 play overlapping roles in promoting rapid F-actin depolymerization in mammalian nonmuscle cells. *Mol. Biol. Cell* **16**, 649-664.

Ichetovkin, I., Grant, W. and Condeelis, J. (2002). Cofilin produces newly polymerized actin filaments that are preferred for dendritic nucleation by the Arp2/3 complex. *Curr. Biol.* **12**, 79-84.

Innocenti, M., Zucconi, A., Disanza, A., Frittoli, E., Areces, L. B., Steffen, A., Stradal, T. E. B., Di Fiore, P. P., Carlier, M.-F. and Scita, G. (2004). Abi1 is essential for the formation and activation of a WAVE2 signalling complex. *Nat. Cell Biol.* **6**, 319-327.

Innocenti, M., Gerboth, S., Rottner, K., Lai, F. P. L., Hertzog, M., Stradal, T. E. B., Frittoli, E., Didry, D., Polo, S., Disanza, A. et al. (2005). Abi1 regulates the activity of N-WASP and WAVE in distinct actin-based processes. *Nat. Cell Biol.* **7**, 969-976.

Insall, R. H. and Machesky, L. M. (2009). Actin dynamics at the leading edge: from simple machinery to complex networks. *Dev. Cell* **17**, 310-322.

Isogai, T., van der Kammen, R., Goerdayal, S. S., Heck, A. J., Altelaar, A. F. and Innocenti, M. (2015a). Proteomic analyses uncover a new function and mode of action for mouse homolog of Diaphanous 2 (mDia2). *Mol. Cell Proteomics.* **14**, 1064-1078.

Isogai, T., van der Kammen, R. and Innocenti, M. (2015b). SMIFH2 has effects on Formins and p53 that perturb the cell cytoskeleton. *Sci. Rep.* **5**, 9802.

Itoh, R. E., Kurokawa, K., Ohba, Y., Yoshizaki, H., Mochizuki, N. and Matsuda, M. (2002). Activation of rac and cdc42 video imaged by fluorescent resonance energy transfer-based single-molecule probes in the membrane of living cells. *Mol. Cell. Biol.* **22**, 6582-6591.

Iwasa, J. H. and Mullins, R. D. (2007). Spatial and temporal relationships between actin-filament nucleation, capping, and disassembly. *Curr. Biol.* **17**, 395-406.

Kim, M.-Y., Oskarsson, T., Acharyya, S., Nguyen, D. X., Zhang, X. H.-F., Norton, L. and Massague, J. (2009). Tumor self-seeding by circulating cancer cells. *Cell* **139**, 1315-1326.

Kovar, D. R., Harris, E. S., Mahaffy, R., Higgs, H. N. and Pollard, T. D. (2006). Control of the assembly of ATP- and ADP-actin by formins and profilin. *Cell* **124**, 423-435.

Kurokawa, K. and Matsuda, M. (2005). Localized RhoA activation as a requirement for the induction of membrane ruffling. *Mol. Biol. Cell* **16**, 4294-4303.

Le Clainche, C. and Carlier, M.-F. (2008). Regulation of actin assembly associated with protrusion and adhesion in cell migration. *Physiol. Rev.* **88**, 489-513.

Lebensohn, A. M. and Kirschner, M. W. (2009). Activation of the WAVE complex by coincident signals controls actin assembly. *Mol. Cell* **36**, 512-524.

Lewkowicz, E., Herit, F., Le Clainche, C., Bourdoncle, P., Perez, F. and Niedergang, F. (2008). The microtubule-binding protein CLIP-170 coordinates mDia1 and actin reorganization during CR3-mediated phagocytosis. *J. Cell Biol.* **183**, 1287-1298.
Machesky, L. M. (2008). Lamellipodia and filopodia in metastasis and invasion. *FEBS Lett.* **582**, 2102-2111.
Maiti, S., Michelot, A., Gould, C., Blanchoin, L., Sokolova, O. and Goode, B. L. (2012). Structure and activity of full-length formin mDia1. *Cytoskeleton* **69**, 393-405.
Mercer, J. and Helenius, A. (2009). Virus entry by macropinocytosis. *Nat. Cell Biol.* **11**, 510-520.
Nobes, C. D. and Hall, A. (1995). Rho, rac, and cdc42 GTPases regulate the assembly of multimolecular focal complexes associated with actin stress fibers, lamellipodia, and filopodia. *Cell* **81**, 53-62.
Nolen, B. J., Tomasevic, N., Russell, A., Pierce, D. W., Jia, Z., McCormick, C. D., Hartman, J., Sakowicz, R. and Pollard, T. D. (2009). Characterization of two classes of small molecule inhibitors of Arp2/3 complex. *Nature* **460**, 1031-1034.
Otomo, T., Otomo, C., Tomchick, D. R., Machius, M. and Rosen, M. K. (2005). Structural basis of Rho GTPase-mediated activation of the formin mDia1. *Mol. Cell* **18**, 273-281.
Pertz, O., Hodgson, L., Klemke, R. L. and Hahn, K. M. (2006). Spatiotemporal dynamics of RhoA activity in migrating cells. *Nature* **440**, 1069-1072.
Pollard, T. D. (2007). Regulation of actin filament assembly by Arp2/3 complex and formins. *Annu. Rev. Biophys. Biomol. Struct.* **36**, 451-477.
Pollard, T. D. and Borisy, G. G. (2003). Cellular motility driven by assembly and disassembly of actin filaments. *Cell* **112**, 453-465.
Rogers, S. L., Wiedemann, U., Stuurman, N. and Vale, R. D. (2003). Molecular requirements for actin-based lamella formation in Drosophila S2 cells. *J. Cell Biol.* **162**, 1079-1088.
Romero, S., Le Clainche, C., Didry, D., Egile, C., Pantaloni, D. and Carlier, M.-F. (2004). Formin is a processive motor that requires profilin to accelerate actin assembly and associated ATP hydrolysis. *Cell* **119**, 419-429.
Rotty, J. D., Wu, C. and Bear, J. E. (2013). New insights into the regulation and cellular functions of the ARP2/3 complex. *Nat. Rev. Mol. Cell Biol.* **14**, 7-12.
Rotty, J. D., Wu, C., Haynes, E. M., Suarez, C., Winkelman, J. D., Johnson, H. E., Haugh, J. M., Kovar, D. R. and Bear, J. E. (2015). Profilin-1 serves as a gatekeeper for actin assembly by Arp2/3-dependent and -independent pathways. *Dev. Cell* **32**, 54-67.
Sakata, D., Taniguchi, H., Yasuda, S., Adachi-Morishima, A., Hamazaki, Y., Nakayama, R., Miki, T., Minato, N. and Narumiya, S. (2007). Impaired T lymphocyte trafficking in mice deficient in an actin-nucleating protein, mDia1. *J. Exp. Med.* **204**, 2031-2038.
Sano, Y., Watanabe, W. and Matsunaga, S. (2014). Chromophore-assisted laser inactivation–towards a spatiotemporal-functional analysis of proteins, and the ablation of chromatin, organelle and cell function. *J. Cell Sci.* **127**, 1621-1629.
Schonichen, A. and Geyer, M. (2010). Fifteen formins for an actin filament: a molecular view on the regulation of human formins. *Biochim. Biophys. Acta* **1803**, 152-163.
Sidani, M., Wessels, D., Mouneimne, G., Ghosh, M., Goswami, S., Sarmiento, C., Wang, W., Kuhl, S., El-Sibai, M., Backer, J. M. et al. (2007). Cofilin determines the migration behavior and turning frequency of metastatic cancer cells. *J. Cell Biol.* **179**, 777-791.
Suarez, C., Carroll, R. T., Burke, T. A., Christensen, J. R., Bestul, A. J., Sees, J. A., James, M. L., Sirotkin, V. and Kovar, D. R. (2015). Profilin regulates F-actin network homeostasis by favoring formin over Arp2/3 complex. *Dev. Cell* **32**, 43-53.
Suetsugu, S., Yamazaki, D., Kurisu, S. and Takenawa, T. (2003). Differential roles of WAVE1 and WAVE2 in dorsal and peripheral ruffle formation for fibroblast cell migration. *Dev. Cell* **5**, 595-609.
Suraneni, P., Rubinstein, B., Unruh, J. R., Durnin, M., Hanein, D. and Li, R. (2012). The Arp2/3 complex is required for lamellipodia extension and directional fibroblast cell migration. *J. Cell Biol.* **197**, 239-251.
Takemoto, K., Matsuda, T., Sakai, N., Fu, D., Noda, M., Uchiyama, S., Kotera, I., Arai, Y., Horiuchi, M., Fukui, K. et al. (2013). SuperNova, a monomeric photosensitizing fluorescent protein for chromophore-assisted light inactivation. *Sci. Rep.* **3**, 2629.
Takenawa, T. and Suetsugu, S. (2007). The WASP-WAVE protein network: connecting the membrane to the cytoskeleton. *Nat. Rev. Mol. Cell Biol.* **8**, 37-48.
Tanizaki, H., Egawa, G., Inaba, K., Honda, T., Nakajima, S., Moniaga, C. S., Otsuka, A., Ishizaki, T., Tomura, M., Watanabe, T. et al. (2010). Rho-mDia1 pathway is required for adhesion, migration, and T-cell stimulation in dendritic cells. *Blood* **116**, 5875-5884.
Vitriol, E. A., Wise, A. L., Berginski, M. E., Bamburg, J. R. and Zheng, J. Q. (2013). Instantaneous inactivation of cofilin reveals its function of F-actin disassembly in lamellipodia. *Mol. Biol. Cell* **24**, 2238-2247.
Wagner, A. R., Luan, Q., Liu, S.-L. and Nolen, B. J. (2013). Dip1 defines a class of Arp2/3 complex activators that function without preformed actin filaments. *Curr. Biol.* **23**, 1990-1998.
Watanabe, N., Madaule, P., Reid, T., Ishizaki, T., Watanabe, G., Kakizuka, A., Saito, Y., Nakao, K., Jockusch, B. M. and Narumiya, S. (1997). p140mDia, a mammalian homolog of Drosophila diaphanous, is a target protein for Rho small GTPase and is a ligand for profilin. *EMBO J.* **16**, 3044-3056.
Watanabe, N., Kato, T., Fujita, A., Ishizaki, T. and Narumiya, S. (1999). Cooperation between mDia1 and ROCK in Rho-induced actin reorganization. *Nat. Cell Biol.* **1**, 136-143.
Yamazaki, D., Suetsugu, S., Miki, H., Kataoka, Y., Nishikawa, S.-I., Fujiwara, T., Yoshida, N. and Takenawa, T. (2003). WAVE2 is required for directed cell migration and cardiovascular development. *Nature* **424**, 452-456.
Yan, C., Martinez-Quiles, N., Eden, S., Shibata, T., Takeshima, F., Shinkura, R., Fujiwara, Y., Bronson, R., Snapper, S. B., Kirschner, M. W. et al. (2003). WAVE2 deficiency reveals distinct roles in embryogenesis and Rac-mediated actin-based motility. *EMBO J.* **22**, 3602-3612.
Zaoui, K., Honore, S., Isnardon, D., Braguer, D. and Badache, A. (2008). Memo-RhoA-mDia1 signaling controls microtubules, the actin network, and adhesion site formation in migrating cells. *J. Cell Biol.* **183**, 401-408.

SUPPLEMENTAL FIGURES

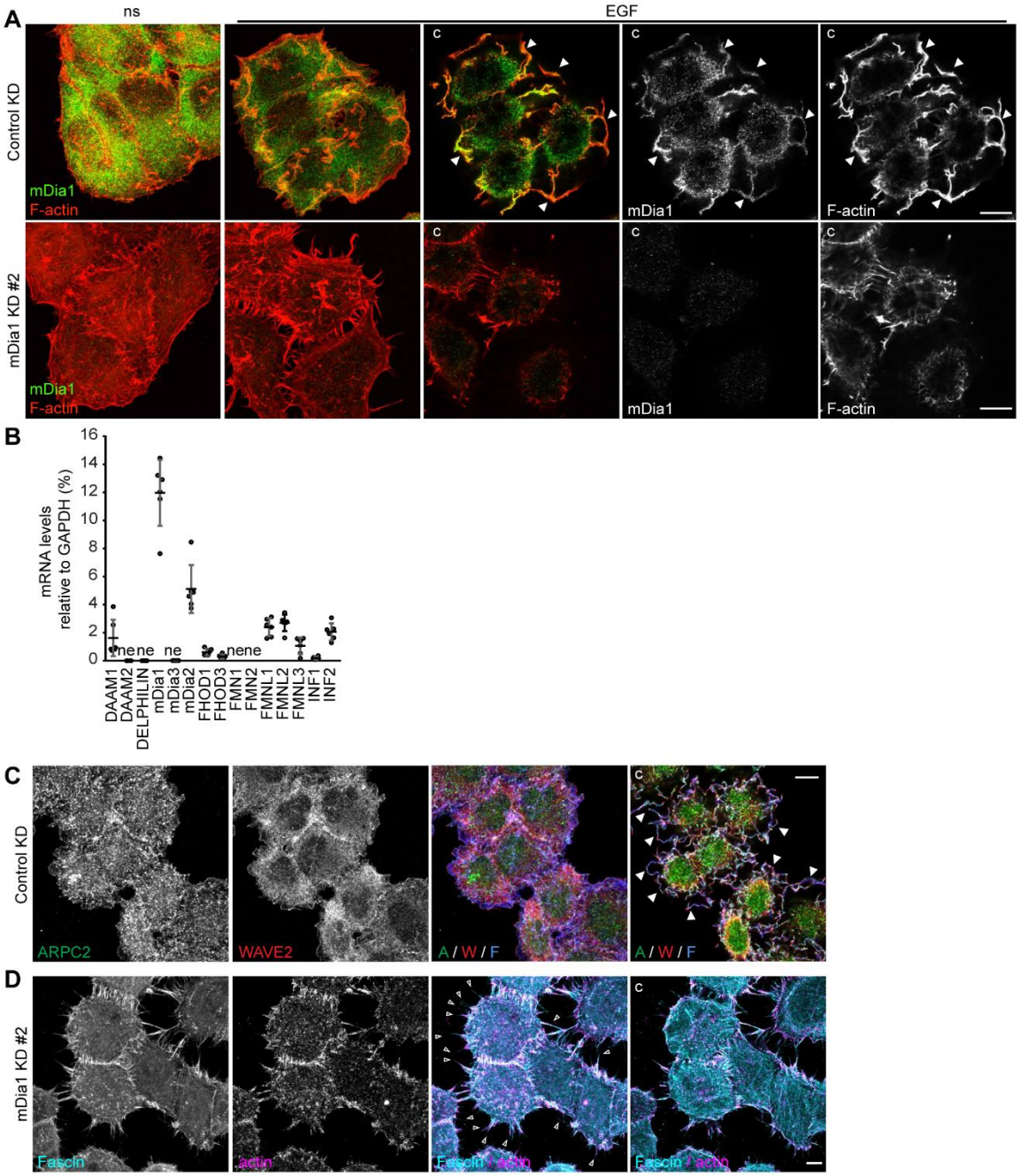

Figure S1. Endogenous mDia1 localizes within EGF-induced ruffles and participates in the formation of ruffles and lamellipodia in multiple cell lines.

(A) Endogenous mDia1 localizes within EGF-induced ruffles. Control (Control KD) and mDia1 knockdown (mDia1 KD #2) HeLa cells were serum-starved (ns) and then either stimulated with EGF (EGF; 100 ng ml-1 for 7 minutes) or left untreated. Fixed cells were stained with anti-mDia1 antibodies (green in merge) and TRITC-phalloidin (red in merge). Representative maximal and central confocal sections (c) of EGF-treated cells are shown. The enrichment of endogenous mDia1 within expanding EGF-induced ruffles was confirmed using EGFP as volumetric marker, as shown in Fig. 3. Similar results were obtained using a different anti-mDia1 antibody (not shown). Note that the comparison between control and mDia1 KD cells demonstrates the specificity of the employed antibodies. White arrowheads mark ruffles. Bar, 10 µm. (B) Formin expression landscape in HeLa cells. Expression of Formins was assessed by RT-qPCR as explained in the Methods starting from total mRNA isolated from exponentially growing HeLa cells. Data are presented as mean ± s.d. of two independent mRNA isolations, each consisting of three technical replicates. *DAAM2, DELPHILIN, mDia3, FMN1* and *FMN2* are not expressed (ne). (C-D) Serum-starved and EGF-stimulated control (Control KD) and mDia1 knockdown (mDia1 KD #2) HeLa cells were fixed and stained with the indicated antibodies. (ARPC2 (A): green in merge; WAVE2 (W): red in merge, and F-actin (F): blue in merge). Representative maximal projections or central confocal sections (c) are presented. As cells were fixed in ice-cold Methanol to enable detection of Fascin with anti-Fascin antibodies (Fascin: false-coloured cyan in merge), anti-actin antibodies were used to label the actin cytoskeleton (actin: false-coloured magenta in merge). Bar, 10 µm.

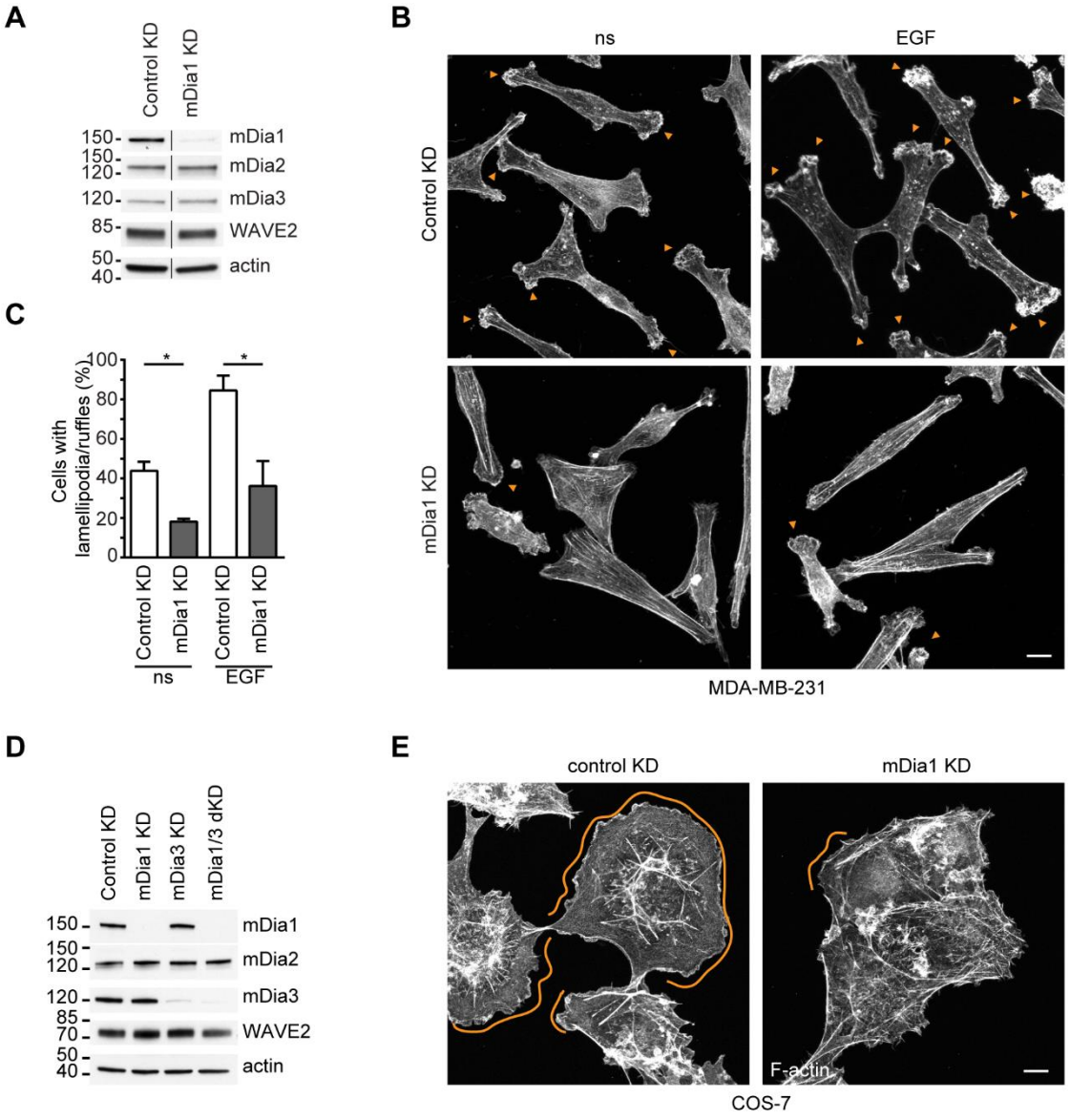

Figure S2. mDia1 participates in the formation of ruffles and lamellipodia also in MDA-MB-231 and COS-7 cells.

(A) Stable control (Control KD) and mDia1 knockdown (mDia1 KD) MDA-MB-231 cells were characterized with the indicated antibodies. One of two experiments that were performed with similar results is shown. (B) Stable control (Control KD) and mDia1 knockdown (mDia1 KD) MDA-MB-231 were plated on collagen-coated coverslips, serum-starved overnight and then either stimulated with EGF (25 ng ml-1) for 7 minutes (EGF) or left untreated (ns). After fixation, cells were stained with TRITC-phalloidin. Representative maximal projections are presented. Orange arrowheads mark ruffles. Bar, 10 µm. (C) Percentage of ruffling cells was quantified for both serum-starved and EGF-stimulated cells. Graph depicts mean ± s.d. (t-test; * = $p < 0.05$; n = 170-177 cells from two independent experiments). (D) Stable control knockdown (Control KD) and mDia1 knockdown (mDia1 KD), mDia3 knockdown (mDia3 KD) or mDia1/mDia3 double knockdown (mDia1/3 dKD) COS-7 cells were characterized with the indicated antibodies. One of two experiments that were performed with similar results is shown. (E) Control and mDia1 knockdown COS-7 cells were plated on fibronectin-coated coverslips, kept in low serum and stained with TRITC-phalloidin. Representative maximal projections are shown. Areas with lamellipodia/ruffles are surrounded by orange lines. Bar, 10 µm. (F) Percentage of ruffling cells was quantified and plotted as mean ± s.d. (One-way ANOVA (Bonferroni's Multiple Comparison Test); ** = $p < 0.01$; n = 171-206 cells from three independent experiments).

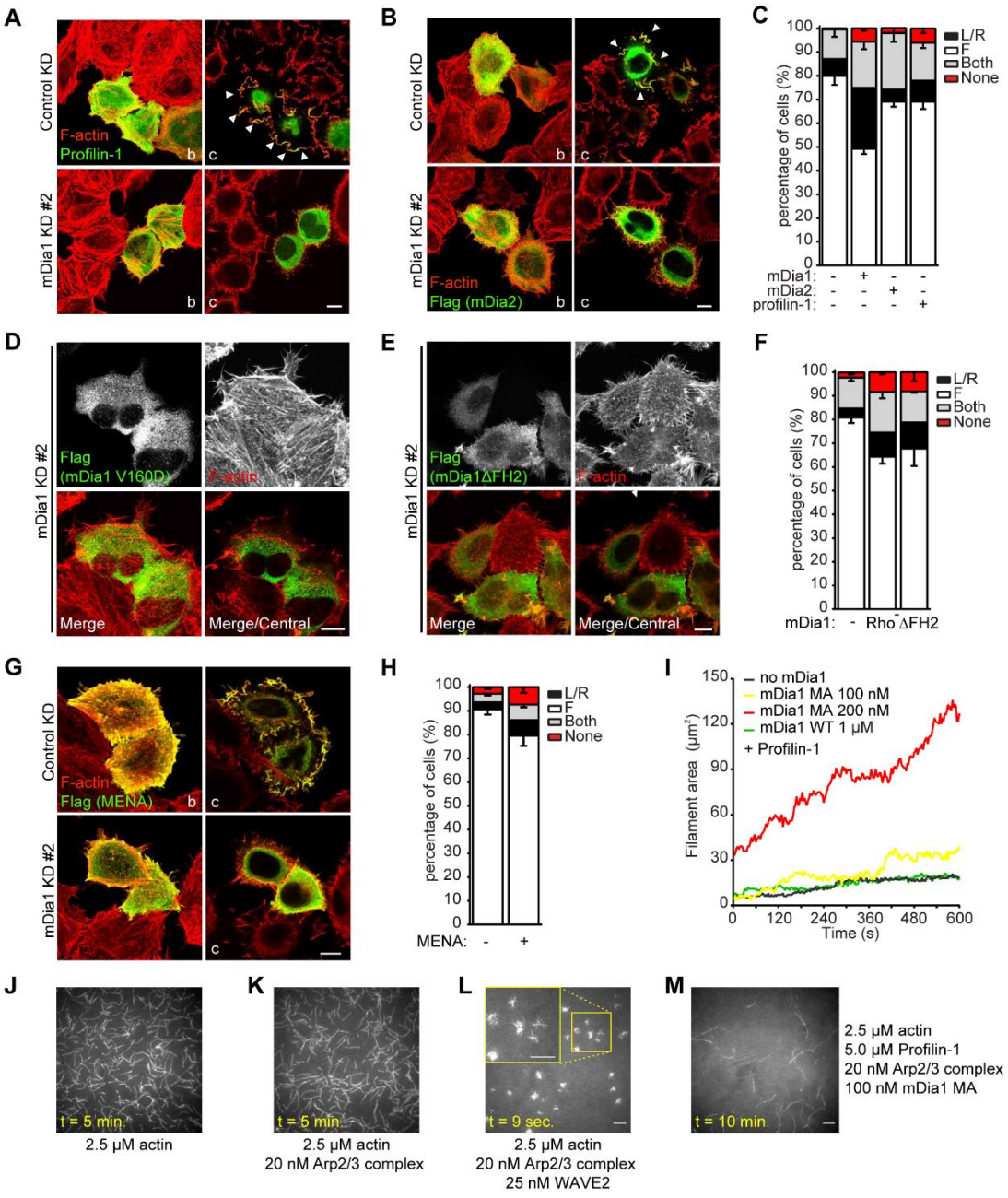

Figure S3. Profilin-1, mDia2, mDia1ΔFH2, mDia1 V160D and Mena did not rescue lamellipodium/ruffle formation in mDia1 KD cells, and mDia1 is an auto-inhibited actin nucleator and does not activate the Arp2/3 complex directly.

(A-C) Overexpression of Profilin-1 and mDia2 fail to rescue lamellipodia/ruffle formation in mDia1 KD cells. Control KD and mDia1 KD #2 cells were transfected with either EGFP-tagged Profilin-1 (A) or Flag-tagged mDia2 (B), serum-starved and stimulated with EGF. After fixation,

exogenous mDia2 was detected using anti-Flag antibodies (green in merge). TRITC-phalloidin (red in merge) was used to detect actin filaments. Representative basal (b) and central confocal sections (c) are shown. White arrowheads mark ruffles. (C) EGF-induced protrusions formed by mDia1 KD cells from (B-C) were quantified as in Fig. 1E. Graph shows mean ± s.e.m. (One-WAY ANOVA; n = 306-308 cells from three independent experiments). Supplementary Material Table S4 shows statistical analysis of these experiments. (D-F) The Rho-binding and the FH2 domain of mDia1 are required for EGF-induced lamellipodium/ruffle formation. mDia1 KD #2 cells were transfected with Flag-tagged mDia1 V160D (D) or Flag-tagged mDia1ΔFH2 (E), and processed as indicated above. (F) EGF-induced protrusions of cells from (D-E) were quantified as in Fig. 1E. (Rho^- = mDia1 V160D; ΔFH2 = mDia1ΔFH2). Graph shows mean ± s.e.m. (One-WAY ANOVA; n = 306-308 cells from three independent experiments). Supplementary Material Table S5 shows statistical analysis of these experiments. (G-H) Mena does not rescue ruffle formation in mDia1 KD cells. mDia1 KD #2 cells were transfected with Flag-tagged Mena and processed as indicated above. (H) EGF-induced protrusions formed by Mena-transfected cells from (G) were quantified as in Fig. 1E. Graph shows mean ± s.e.m. (One-WAY ANOVA; n > 200 cells from two independent experiments). Supplementary Material Table S6 shows statistical analysis of these experiments. All bars, 10 µm. (I) mDia1 MA is an auto-inhibited actin nucleator. Actin (2.5 µM) was polymerized in the presence of Profilin-1 either alone or in with the indicated concentrations of mDia1 WT or mDia1 MA. Area filled with actin filaments was quantified using representative movies as described in Materials and Methods. (J-L) The Arp2/3 complex is unable to form branches in the absence of WAVE2. Actin was polymerized either alone (I) or in the presence of the Arp2/3 complexes with or without WAVE2 (K and L, respectively). Conditions are indicated below the micrographs (t = time; min. = minutes; sec. = seconds). Bars, 10 µm. (M) mDia1 does not activate the Arp2/3 complex directly. Actin was polymerized in the presence of Profilin-1, the Arp2/3 complex and mDia1 MA, but without WAVE2. Conditions are indicated beside the micrograph (t = time; min. = minutes). Bar 10 µm.

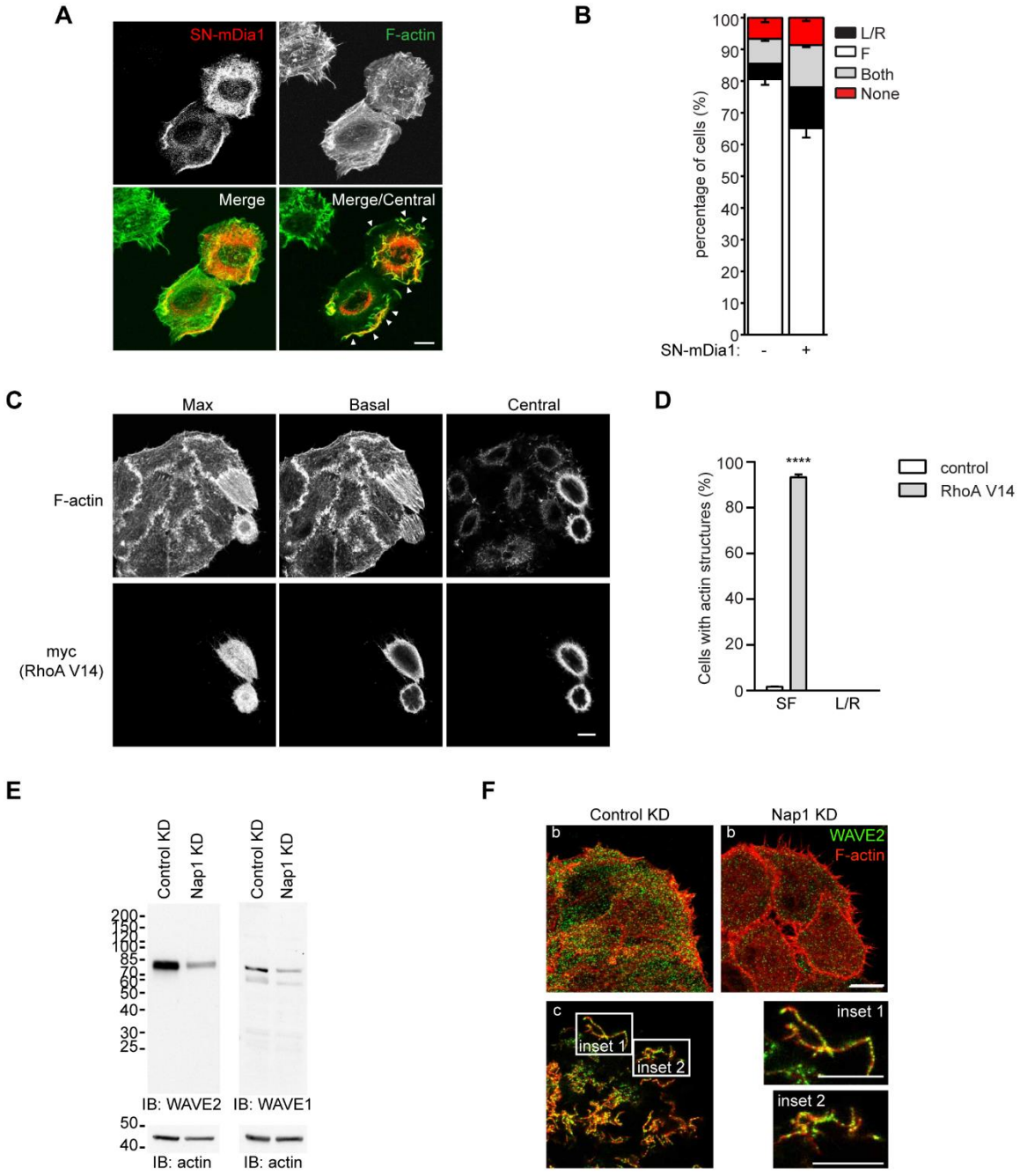

Figure S4. SuperNova-mDia1 rescues EGF-induced ruffling in mDia1 KD cells, constitutively active Rho is insufficient to induce lamellipodia/ruffles, and characterization of anti-WAVE2 antibodies.

(A-B) mDia1 KD #2 cells were transfected with SuperNova-mDia1 (SN-mDia1), serum-starved and stimulated with EGF (100 ng ml^{-1}; 7 minutes). After fixation, cells were stained with anti-KillerRed antibodies (red in merge) and FITC-phalloidin (green in merge) to detect SuperNova-mDia1 and actin filaments, respectively. Representative maximal projections and central confocal sections (Merge/Central) are shown. White arrowheads mark lamellipodia and ruffles. Bar, 10 µm. B: EGF-induced protrusions of cells from (A) were quantified as in Fig. 1E. Graph shows mean ± s.e.m. (One-WAY ANOVA; $n \geq 400$ cells from three independent experiments). Supplementary Material Table S7 shows statistical analysis of these experiments. (C) Wild-type HeLa cells were transfected with myc-tagged constitutively active RhoA (RhoA V14), serum starved and fixed. After fixation, cells were stained with anti-myc antibodies and TRITC-phalloidin to detect RhoA V14 and actin filaments, respectively. Representative maximal projections and central confocal sections (Merge/Central) are shown. Bar, 10 µm. (D) Cells from (A) were quantified for increased stress-fiber (SF) formation and lamellipodia/ruffle (L/R) formation. Graph shows mean ± s.e.m. (t-test; **** = $p < 0.0001$; $n \geq 300$ cells from three independent experiments). No lamellipodia/ruffles were observed in three independent experiments. (E) Specificity of anti-WAVE2 antibodies. Total cell lysates obtained from control and Nap1 knockdown cells were blotted with anti-WAVE2, anti WAVE1 and anti-actin antibodies. Note that the anti-WAVE2 antibodies detect a single species whose intensity decreases upon silencing of Nap1. Consistent with the downregulation of the WAVE complex in Nap1 KD cells, the expression of WAVE1 was also reduced in these cells. (F) Specificity of anti-WAVE2 antibodies and localization of endogenous WAVE2. Control and Nap1 knockdown cells were stimulated with EGF (100 ng ml^{-1}) for 7 minutes, processed and stained with anti-WAVE2 antibodies (green in the merge) and TRITC-Phalloidin (red in the merge). Basal (b) and central confocal sections (c) of EGF-treated cells are shown. Insets (1 and 2) zoom in to the localization of endogenous WAVE2 within two different ruffling area. Bars, 10 µm.

SUPPLEMENTAL MOVIES

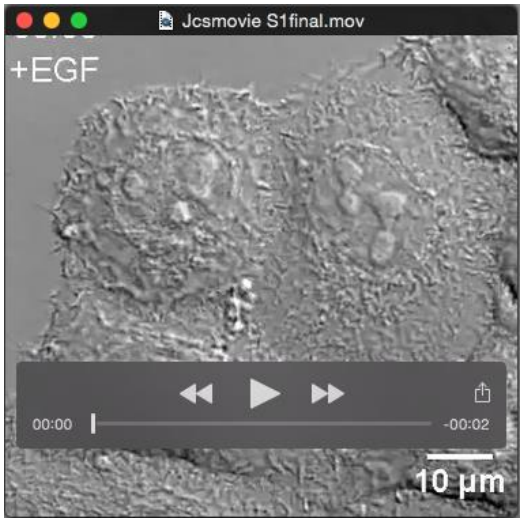

Movie 1

Control HeLa cells form dynamic lamellipodium-like and ruffle-like protrusions upon EGF stimulation. Images were acquired every 15 seconds.

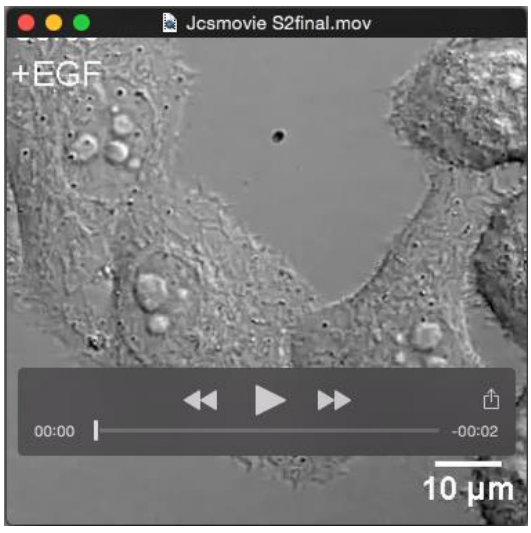

Movie 2

mDia1 KD #2 HeLa cells form dynamic filopodium-like protrusions growing by extension upon EGF stimulation. Images were acquired every 15 seconds and acquired in parallel to Movie 1.

Movie 3

mDia1 WT is an auto-inhibited Formin. Profilin-actin was polymerized in the absence or presence of 1 μM of mDia1 WT. Imaging was carried out as described in the Materials and Methods.

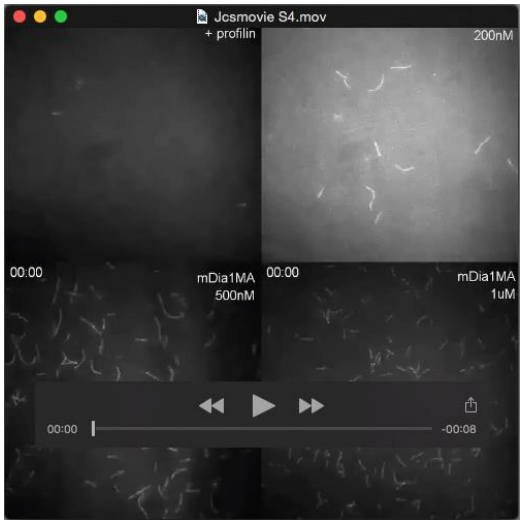

Movie 4

mDia1 MA nucleates and elongates actin filaments in the presence of Profilin-1. Profilin-bound actin was polymerized in the absence or presence of indicated concentration of mDia1 MA. Imaging was carried out as described in the Materials and Methods.

Movie 5

mDia1 polymerizes linear actin filaments activating the Arp2/3 complex. A reaction containing profilin-actin, full-length 25 nM WAVE2 and 20 nM Arp2/3 complex was polymerized in the absence or presence of indicated concentration of mDia1 MA. Imaging was carried out as described in the Materials and Methods.

Movie 6

Demonstration of the effectiveness of Chromophore-Assisted Laser Inactivation (CALI) of SuperNova-mDia1. mDia1 knockdown #2 HeLa cells were transiently transfected with SuperNova-mDia1 and serum starved overnight. Chromophore-Assisted Laser Inactivation (CALI) was performed prior to addition of EGF (100 ng ml^{-1}). Images were acquired every 5 seconds. Arrows highlight lamellipodia/ruffles. Note that CALI of SN-mDia1 prevented ruffling. Bar, 10 µm.

Movie 7

mDia1 is dispensable for expansion of lamellipodia/ruffles. mDia1 knockdown #2 HeLa cells were transiently transfected with SuperNova-mDia1, serum starved overnight and stimulated 3 minutes with EGF (100 ng ml^{-1}) prior to Chromophore-Assisted Laser Inactivation (CALI). Images were acquired every 5 seconds. Arrows highlight lamellipodia/ruffles. Note that CALI of SN-mDia1 did not stop ruffling. Bar, 10 µm.

Table S1 - Statistical analysis corresponding to Figure 1E

Bonferroni's multiple comparisons test	Mean Difference	Significant?	Summary	Adj. P Value
Filopodia				
shControl *vs.* shDIAPH1 #1	-51.9	Yes	****	< 0,0001
shControl *vs.* shDIAPH1 #2	-75.6	Yes	****	< 0,0001
Ruffling/Lamellipodia				
shControl *vs.* shDIAPH1 #1	74.8	Yes	****	< 0,0001
shControl *vs.* shDIAPH1 #2	81.17	Yes	****	< 0,0001
Both				
shControl *vs.* shDIAPH1 #1	-14.4	Yes	***	0.0007
shControl *vs.* shDIAPH1 #2	2.233	No	ns	> 0,9999
None				
shControl *vs.* shDIAPH1 #1	-8.567	Yes	*	0.0422
shControl *vs.* shDIAPH1 #2	-7.733	No	ns	0.071

One-WAY ANOVA (Bonferroni's Multiple Comparison Test; * = $p < 0.05$; *** = $p < 0.001$; **** = $p < 0.0001$; $n \geq 300$ cells from three independent experiments).

Table S2 - Statistical analysis corresponding to Figure 2B

Bonferroni's multiple comparisons test	Mean Difference	Significant?	Summary	Adj. P Value
Filopodia				
shDIAPH1 #1 *vs.* shDIAPH1 #1 + mDia1	20.73	Yes	**	0.0025
shDIAPH1 #2 *vs.* shDIAPH1 #2 + mDia1	27.17	Yes	***	0.0002
Ruffling/Lamellipodia				
shDIAPH1 #1 *vs.* shDIAPH1 #1 + mDia1	-19.50	Yes	**	0.0042
shDIAPH1 #2 *vs.* shDIAPH1 #2 + mDia1	-17.73	Yes	*	0.0207
Both				
shDIAPH1 #1 *vs.* shDIAPH1 #1 + mDia1	-2.000	No	ns	> 0.9999
shDIAPH1 #2 vs. shDIAPH1 #2 + mDia1	-7.733	No	ns	> 0.9999
None				
shDIAPH1 #1 *vs.* shDIAPH1 #1 + mDia1	0.7667	No	ns	> 0.9999
shDIAPH1 #2 *vs.* shDIAPH1 #2 + mDia1	-1.767	No	ns	> 0.9999

One-WAY ANOVA (Bonferroni's Multiple Comparison Test; * = $p < 0.05$; ** = $p < 0.01$; *** = $p < 0.001$; $n \geq 300$ cells from three independent experiments).

Table S3 - Statistical analysis of membrane protrusions formed by control KD HeLa cells overexpressing mDia1 compared to non-transfected ones

Bonferroni's multiple comparisons test	Mean Difference	Significant?	Summary	Adj. P Value
Filopodia	-1.283	No	ns	0.9819
Ruffling/Lamellipodia	7.075	No	ns	0.0909
Both	-1.108	No	ns	0.9895
None	-4.675	No	ns	0.3603

One-WAY ANOVA (Bonferroni's Multiple Comparison Test; * = $p < 0.05$; **** = $p < 0.0001$; $n \geq 200$ cells from four independent experiments).

Table S4 - Statistical analysis corresponding to Figure S3C

Bonferroni's multiple comparisons test	Mean Difference	Significant?	Summary	Adj. P Value
Filopodia				
shDIAPH1 #2 *vs.* shDIAPH1 #2 + mDia1	30.80	Yes	****	< 0.0001
shDIAPH1 #2 *vs.* shDIAPH1 #2 + mDia2	10.90	Yes	*	0.0124
shDIAPH1 #2 *vs.* shDIAPH1 #2 + Profilin-1	10.90	Yes	*	0.0124
Ruffling/Lamellipodia				
shDIAPH1 #2 *vs.* shDIAPH1 #2 + mDia1	-18.60	Yes	****	< 0.0001
shDIAPH1 #2 *vs.* shDIAPH1 #2 + mDia2	1.967	No	ns	> 0.9999
shDIAPH1 #2 *vs.* shDIAPH1 #2 + Profilin-1	-1.733	No	ns	> 0.9999
Both				
shDIAPH1 #2 *vs.* shDIAPH1 #2 + mDia1	-7.000	No	ns	0.1678
shDIAPH1 #2 *vs.* shDIAPH1 #2 + mDia2	-11.33	Yes	**	0.0090
shDIAPH1 #2 *vs.* shDIAPH1 #2 + Profilin-1	-3.500	No	ns	0.9862
None				
shDIAPH1 #2 *vs.* shDIAPH1 #2 + mDia1	-5.200	No	ns	0.4511
shDIAPH1 #2 *vs.* shDIAPH1 #2 + mDia2	-1.667	No	ns	> 0.9999
shDIAPH1 #2 *vs.* shDIAPH1 #2 + Profilin-1	-5.600	No	ns	0.3671

One-WAY ANOVA (Bonferroni's Multiple Comparison Test; * = $p < 0.05$; ** = $p < 0.01$; **** = $p < 0.0001$; $n \geq 300$ cells from three independent experiments).

Table S5 - Statistical analysis corresponding to Figure S3F

Bonferroni's multiple comparisons test	Mean Difference	Significant?	Summary	Adj. P Value
Filopodia				
shDIAPH1 #2 *vs.* shDIAPH1 #2 + V160D-mDia1	13.22	Yes	***	0.0008
shDIAPH1 #2 *vs.* shDIAPH1 #2 + mDia1ΔFH2	16.65	Yes	****	< 0.0001
Ruffling/Lamellipodia				
shDIAPH1 #2 vs. shDIAPH1 #2 + V160D-mDia1	-7.183	No	ns	0.0834
shDIAPH1 #2 *vs.* shDIAPH1 #2 + mDia1ΔFH2	-6.283	No	ns	0.1459
Both				
shDIAPH1 #2 vs. shDIAPH1 #2 + V160D-mDia1	-0.06667	No	ns	> 0.9999
shDIAPH1 #2 *vs.* shDIAPH1 #2 + mDia1ΔFH2	-4.200	No	ns	0.4498
None				
shDIAPH1 #2 vs. shDIAPH1 #2 + V160D-mDia1	-5.967	No	ns	0.1758
shDIAPH1 #2 *vs.* shDIAPH1 #2 + mDia1ΔFH2	-6.167	No	ns	0.1563

One-WAY ANOVA (Bonferroni's Multiple Comparison Test; * = $p < 0.05$; ** = $p < 0.01$; *** = $p < 0.001$; $n \geq 300$ cells from three independent experiments).

Table S6 - Statistical analysis corresponding to Figure S3H

Bonferroni's multiple comparisons test	Mean Difference	Significant?	Summary	Adj. P Value
Filopodia	11.07	Yes	**	0.0061
Ruffling/Lamellipodia	-3.567	No	ns	0.9457
Both	-2.900	No	ns	> 0.9999
None	-4.600	No	ns	0.5287

One-WAY ANOVA (Bonferroni's Multiple Comparison Test; * = $p < 0.05$; **** = $p < 0.0001$; $n \geq 300$ cells from three independent experiments).

Table S7 - Statistical analysis corresponding to Figure S4B

Bonferroni's multiple comparisons test	Mean Difference	Significant?	Summary	Adj. P Value
Filopodia	15.43	Yes	****	< 0.0001
Ruffling/Lamellipodia	-8.025	Yes	*	0.0104
Both	-5.400	No	ns	0.1324
None	-2.050	No	ns	> 0.9999

One-WAY ANOVA (Bonferroni's Multiple Comparison Test; * = $p < 0.05$; **** = $p < 0.0001$; $n \geq 400$ cells from four independent experiments).

Table S8 - Summary of optogenetic manipulation of SuperNova-mDia1

Percentage of SN-mDia1 expressing cells that underwent CALI prior to EGF stimulation and ruffled	Percentage of SN-mDia1 expressing cells that ruffled upon EGF stimulation	Percentage of SN-mDia1 expressing cells that underwent CALI after EGF stimulation and ruffled
13.8% (5/36)	26.2% (17/63)	28.1% (16 / 57)

Summary of the CALI experiments showing percentage of SuperNova-mDia1-expressing cells that formed EGF-induced lamellipodia/ruffles, as assessed by live-imaging. Data represents cells imaged from three to four independent experiments imaged on different days. Note that percentage of SN-mDia1-expressiong cells subjected to CALI prior to EGF stimulation is similar to the percentage of ruffling observed in Fig. 1E, thereby showing the effective inactivation of SN-mDia1.

Table S9 - Statistical analysis corresponding to Figure 6E

Bonferroni's multiple comparisons test	Mean Difference	Significant?	Summary	Adj. P Value
Filopodia	19.1	Yes	****	< 0,0001
Ruffling/Lamellipodia	-5.067	Yes	*	0.0235
Both	-9.433	Yes	****	< 0,0001
None	-4.6	Yes	*	0.0433

One-WAY ANOVA (Bonferroni's Multiple Comparison Test; * = $p < 0.05$; **** = $p < 0.0001$; $n \geq 150$ cells from three independent experiments).

Table S10 - Primer sequences used for PCR amplification

Construct name	Primer 1 (5'-3')	Primer 2 (5'-3')
Profilin-1	CGGGATCCGCCGGGTGGAACGCCTAC	CGGAATTCTCAGTACTGGGAACGCCG
V160D mDia1	GTCCCTTCGAGACTCTCTCAACAATAA	TCAAGGCAGCTAAGCAGGTG
mDia1 MA	GACAGGTGTGGCGGACAGTCTTC	GAAGACTGTCCGCCACACCTGTC
mDIa1ΔFH2	GAGGGGGATGAGACAGGTG	GGTTAATCCAAATGGCAGAACTGG
SN-mDia1	AACCGGTCGCCACCATGGGTTCAGAGG	AAAGATCTGAGTCCGGAATCCTCGTC GCTACCGATGGC